# BAGOT'S PARK, ABBOTS BROMLEY, STAFFORDSHIRE, II:
## Archaeomagnetic Dating Report 2001

Paul Linford and Chris Welch

**Summary**

Study of the remains of glassmaking sites at Bagot's Park near Abbots Bromley in Staffordshire, has revealed the presence of eighteen furnaces dating from the medieval and post-medieval period. As part of an ongoing project to investigate the evolution of glassmaking in the area, the *CfA* was asked to provide archaeomagnetic dates for the last use of each furnace. Six furnaces were excavated and dated in 2000 and are the subject of a previous report (Linford 2001). A further six furnaces were excavated during 2001 and this report details their archaeomagnetic analysis. Despite most of the structure of the furnaces having been destroyed in the 1960's, it was possible to produce dates of good precision for five of the furnaces. Remains of the sixth had been badly damaged by ploughing and it was not possible to infer an archaeomagnetic date. Now that twelve furnaces have been analysed, some trends in the development of glassmaking at the site begin to emerge.

# BAGOT'S PARK, ABBOTS BROMLEY, STAFFORDSHIRE, II:
## Archaeomagnetic Dating Report 2001

## Introduction

Until the mid-1960s Bagot's Park near Abbots Bromley in Staffordshire (SK 095 275, longitude 1.9°W, latitude 52.8°N) was an area of ancient oak trees and scrubby grazing. A programme of reclamation then ensued to convert the area into productive arable land, during which the remains of a number of glassmaking sites were recognised. One of these (now known as site 4) was excavated by David Crossley in 1966 (Crossley, 1967). He went on to identify a further 14 sites within the Park, although these were not excavated. Unfortunately, the upstanding remains of the furnaces were destroyed during the reclamation using explosives and bulldozers to remove obstacles to ploughing.

No further investigation was carried out until 1996 when Dr. Chris Welch, the county archaeologist for Staffordshire, revisited Bagot's Park. As a result of his investigations a total of eighteen glassmaking sites have been identified within the Park dating from a period between about 1300 and 1615 AD. Dr. Welch has now instigated a project to investigate the evolution of glassmaking in Bagot's Park concentrating on: fieldwalking of the glass making sites (with the assistance of students from Keele University's Staffordshire Archaeology Summer School); geophysical survey (with the assistance of Dr. Ruth Murdie of Keele University); and limited excavation to obtain samples for archaeomagnetic dating (Welch 1998). The latter is essential to establish an absolute chronology for various sites within the Park against which developments in the technology of glassmaking that they exhibit can be measured. Hence, with the support of the English Heritage regional Inspector of Ancient Monuments, Paul Stamper, the Centre for Archaeology (EH C*f*A) was asked to provide archaeomagnetic dates for the features.

As Bagot's Park is under an arable management regime, it is only possible to excavate the glassmaking sites during a few weeks in late summer between the harvesting of one crop and the sowing of the next. Even during this time, the glassmaking sites are not all free of crops simultaneously. The largely volunteer excavation team can only spare a limited amount of time each year for the project, so it was decided to mount several campaigns to collect archaeomagnetic samples over successive years. An initial programme of fieldwork was carried out in September 2000 and is the subject of a previous C*f*A report (Linford 2001). The present report describes the results of further excavations carried out between the 3rd and 6th September 2001.

Six glassmaking sites were excavated in 2001 and in all cases it was found that most of the actual furnace remains had been destroyed when the land was reclaimed in the 1960s. What survived was fired clay that had originally lain beneath the furnaces and, in some cases, a few of the sandstone blocks that comprised the footings of the furnaces. These latter were heavily decayed owing to exposure to intense heat during the furnaces' operation. In two cases (sites 13c and 15a) a residue of the mixture of ground pebbles and bracken used to make the glass was also found *in situ*. However, in all cases there was a limited resource of material that could confidently be identified as undisturbed and well fired, reducing the opportunities for obtaining precise archaeomagnetic dates.

All the archaeomagnetic sampling was carried out by Paul Linford as was the subsequent laboratory measurement and analysis.

## Method

Samples were collected from glassmaking sites 6b, 13a-c, and 15a-b using the disc method (see appendix, section 1a). Samples from site 13c were orientated to true north using a gyro-theodolite. The samples from the other sites were orientated using a magnetic compass, the deviation between magnetic and true north in the area having been established when the gyro-theodolite was used. To identify which glassmaking site each sample came from, all the samples numbers were prefixed by the relevant site number followed by the letters "BP" (e.g.: all samples from site 13c were prefixed with "13CBP").

The natural remanent magnetisation (NRM) measured in archaeomagnetic samples is assumed to be caused by thermoremanent magnetisation (TRM) created at the time when the feature of which they were part was last fired. However, a secondary component acquired in later geomagnetic fields can also be present, caused by diagenesis or partial reheating. Additionally, the primary TRM may be overprinted by a viscous component, depending on the grain size distribution within the magnetic material. These secondary components are usually of lower stability than the primary TRM and can thus be removed by partial demagnetisation of the samples.

A typical strategy for analysing a set archaeomagnetic samples from a fired archaeological feature is to first measure their NRM magnetisation. These NRM measurements are then inspected and one or more samples are selected for pilot partial demagnetisation. Pilot demagnetisation of a sample involves exposing it to an alternating magnetic field of fixed peak strength and measuring the resulting changes in its magnetisation. The procedure is repeated with increasing peak field strengths to build up a complete picture of the coercivity spectrum of the pilot sample. From these pilot partial demagnetisation results an optimum peak field strength is selected to be applied to the remaining samples. This optimum field strength is chosen to remove as much of the secondary magnetisation as possible whilst leaving the primary magnetisation intact. The equipment used for these measurements is described in section 2 of the appendix.

A mean TRM direction is then calculated from the partially demagnetised sample measurements. Some samples may be excluded from this calculation if their TRM directions are so anomalous as to make them statistical outliers from the overall TRM distribution. A "magnetic refraction" correction is often applied to the sample mean TRM direction to compensate for distortion of the earth's magnetic field due to the geometry of the magnetic fabric of the feature itself. Then the mean is adjusted according to the location of the feature relative to a notional central point in the UK (Meriden), so that it can be compared with UK archaeomagnetic calibration data to produce a date of last firing for the feature. Notes concerning the mean calculation and subsequent calibration can be found in sections 3 and 4 of the appendix.

This measurement and calibration strategy was applied to the analysis of the samples from Bagot's Park. As all the samples were taken from the floors of features, a magnetic refraction

correction (Aitken and Hawley, 1971) of 2.4$^o$ was added to the inclination of each mean TRM direction before calibration.

## Results

| Feature | N | Dec$^o$ | Inc$^o$ | $\alpha_{95}$ | k | Date Range | Comment* |
|---|---|---|---|---|---|---|---|
| 6b | 11 | 6.8 (6.8) | 61.0 (60.7) | 3.8 | 145.5 | 63%: 1445 – 1500 AD<br>95%: 1410 – 1520 AD | Assumed contemporary with 6a. Absence of brick suggests a date before 1500. |
| 13a | 12 | 4.8 (4.8) | 57.1 (56.8) | 3.9 | 126.7 | 63%: 1395 – 1445 AD<br>95%: 1380 – 1480 AD | Absence of brick and lack of glass or other finds suggests a medieval date. |
| 13b | 17 | -1.1 (-1.0) | 56.7 (56.3) | 2.4 | 230.6 | 63%: 1380 – 1400 AD<br>95%: 1370 – 1415 AD | As 13a above. |
| 13c | 17 | 10.2 (10.1) | 67.2 (67.0) | 1.9 | 353.1 | 63%: 1530 – 1550 AD<br>95%: 1525 – 1565 AD | As 13a & b. Glasspot found during excavation dissimilar to Wolseley, so contemporary mid C16$^{th}$ date unexpected. |
| 15a | 13 | 2.8 (2.8) | 61.3 (61.0) | 2.2 | 350.3 | 63%: 1280 – 1305 AD<br>95%: 1270 – 1320 AD | Pottery excavated from ditch enclosing feature dates from C11$^{th}$ – C14$^{th}$ AD. |
| 15b | - | - | - | - | - | Undatable | Proximity to remains of C16$^{th}$ AD dwelling suggest a contemporary date. |

*Table 1; Archaeomagnetic dates inferred for features excavated at Bagot's Park in 2001. N = number of samples used to calculate mean TRM. Dec = mean declination (bracketed value is Meriden corrected). Inc = mean inclination (bracketed value is Meriden corrected). $\alpha_{95}$ = internal angle of cone of confidence. k = Fisher precision statistic. *Comment on expected date based upon archaeological considerations.*

Table 1 summarises the mean TRM directions and the inferred date ranges for all the features sampled at Bagot's Park in September 2001. This section provides descriptions of the features sampled and notes any important points about their archaeomagnetic analysis. TRM measurements for all samples may be found grouped by feature in the tables at the end of the report. These tables also record each sample's composition, the demagnetisation level applied to it and whether it was rejected from the feature's mean TRM calculation.
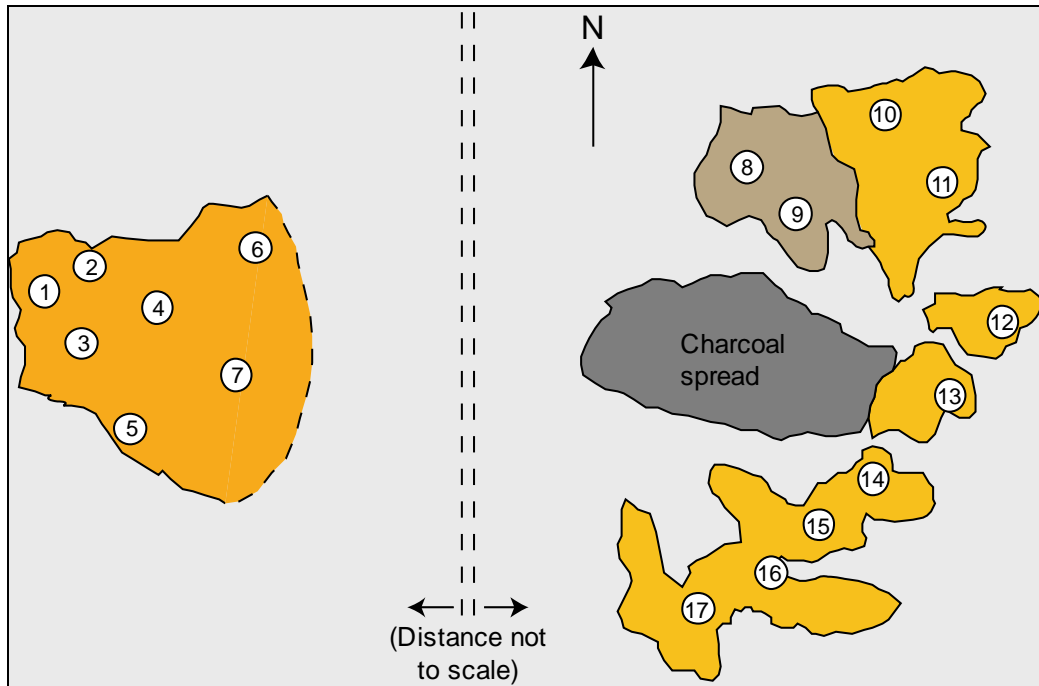
*Figure 1: Sketch plan showing distribution of samples on fired clay areas at site 6b (not to scale).*

*Site 6b*

Heated clay remains beneath this furnace appeared to be somewhat better preserved than at the adjacent site 6a excavated in 2000, although some disturbance due to deep ploughing was evident. Approximate sample locations are depicted in Figure 1 and sample measurements are recorded in Tables 2 and 3. Figure 8 depicts the distribution of sample TRM directions before and after partial demagnetisation. Figures 9 and 10 illustrate the results of pilot demagnetisation on samples 6BBP02 and 6BBP13 respectively (pilot demagnetisation was also carried out on 6BBP09). The magnetisation direction of sample 6BBP02 appeared less stable than that of 6BBP13, suggesting that the area containing samples 6BBP01-07 had been exposed to less intense heat.  For this reason, samples 6BBP01-2 and 6BBP04-5, which exhibited anomalous TRM directions, were rejected. Samples 6BBP09 and 6BBP17 were also rejected as, whilst stable, they appeared to have been disturbed by deep ploughing. Figure 11 shows the comparison of the calculated mean TRM vector with the UK archaeomagnetic calibration curve.
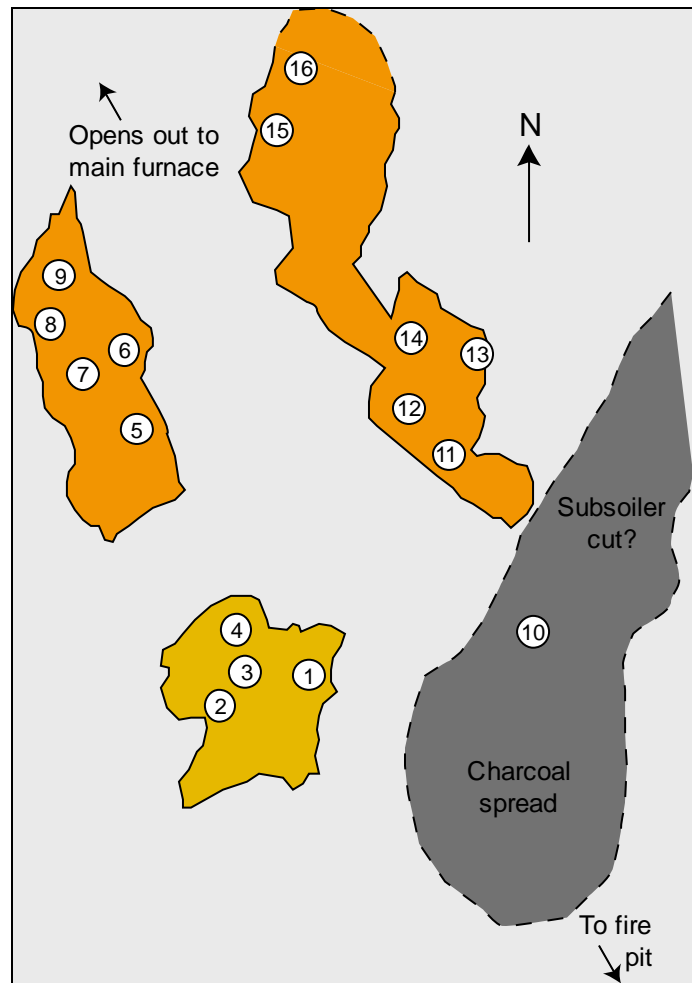
*Figure 2: Sketch plan showing distribution of samples on fired clay areas at site 13a (not to scale).*

*Site 13a*

Heated clay remains here showed evidence of scoring as a result of deep ploughing in this field. Approximate sample locations are depicted in Figure 2 and sample measurements are recorded in Tables 4 and 5. Figure 12 depicts the distribution of sample TRM directions before and after partial demagnetisation. Figure 13 illustrates the results of pilot demagnetisation on sample 13ABP06 (pilot demagnetisation was also carried out on samples 13ABP04 and 13). The magnetisation directions of these samples were stable with some viscous realignment in domains with coercivities below 5mT. Samples 13ABP08, 09 and 12 were very small samples and were thus rejected as unreliable. Further inspection of the feature revealed that sample 13ABP10 had been taken from a groove caused by deep ploughing. Thus it had been disturbed and was rejected. Figure 14 shows the comparison of the calculated mean TRM vector with the UK archaeomagnetic calibration curve.
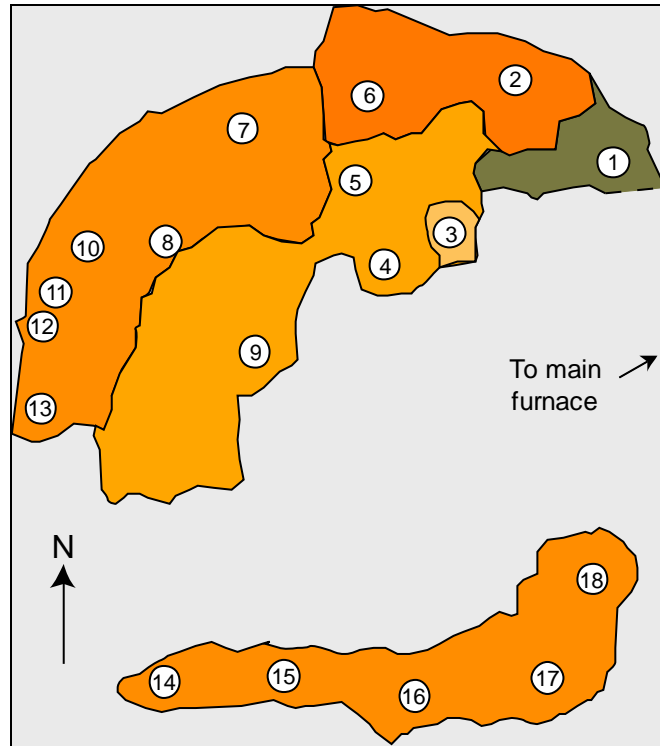
*Figure 3: Sketch plan showing distribution of samples on fired clay areas at site 13b (not to scale).*

*Site 13b*

This feature had been partially damaged by the roots of a tree, which was removed in the 1960s. Approximate sample locations are depicted in Figure 3 and sample measurements are recorded in Tables 6 and 7. Figure 15 depicts the distribution of sample TRM directions before and after partial demagnetisation. Figures 16 and 17 illustrate the results of pilot demagnetisation on samples 13BBP01 and 08 respectively. The magnetisation directions of these samples were stable with some viscous realignment in domains with coercivities below 10mT. Sample 13BBP01 was of a much darker coloration than the other samples and its magnetisation was extremely hard (its median destructive field was of the order of 60mT compared with 30mT for sample 08). Its magnetisation direction was slightly anomalous compared to the other samples, possibly due to this difference in magnetic fabric. It was thus rejected from the mean calculation. Figure 18 shows the comparison of the calculated mean TRM vector with the UK archaeomagnetic calibration curve.
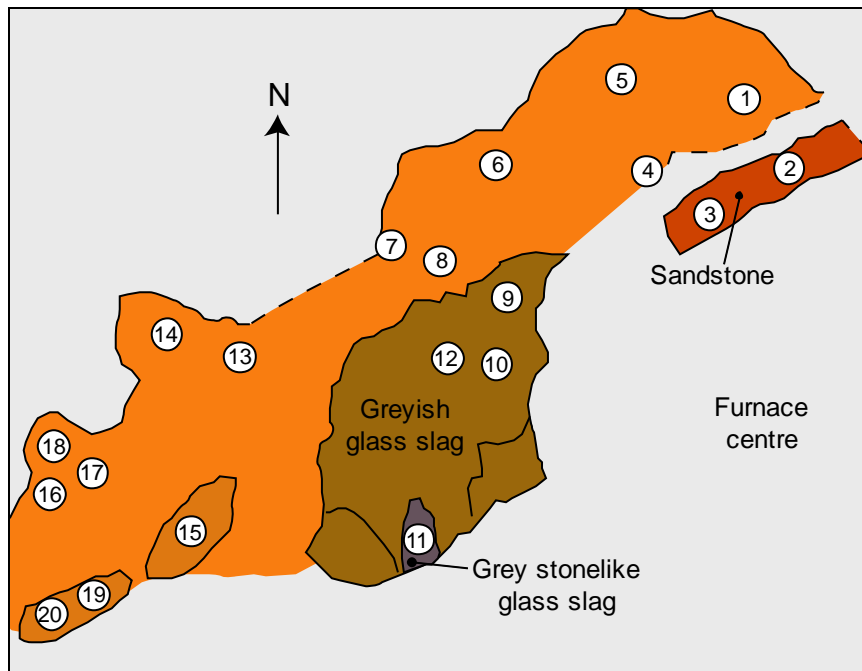
*Figure 4: Sketch plan showing distribution of samples on fired clay areas at site 13c (not to scale).*

*Site 13c*

Heated clay remains here were in relatively good condition with some sandstone and glassmaking slag surviving. Approximate sample locations are depicted in Figure 4 and sample measurements are recorded in Tables 8, 9 and 10. Figure 19 depicts the distribution of sample TRM directions before and after partial demagnetisation. Figures 20, 21 and 22 illustrate the results of pilot demagnetisation on sample 13CBP02, 08 and 11 respectively (pilot demagnetisation was also carried out on samples 13ABP05, 12 and 13). The magnetisation directions of these samples were stable with some viscous realignment in domains with coercivities below 10mT. Samples 13CBP11 exhibited extremely hard magnetisation but with some instability in direction in domains with coercivities below 50mT, hence it was partially demagnetised to 50 rather than 10mT. Samples 13CBP05, 06 and 13 had anomalous directions of magnetisation. It was concluded that this was due to disturbance as these samples were from the outer edge of the feature and they were rejected. Figure 23 shows the comparison of the calculated mean TRM vector with the UK archaeomagnetic calibration curve.
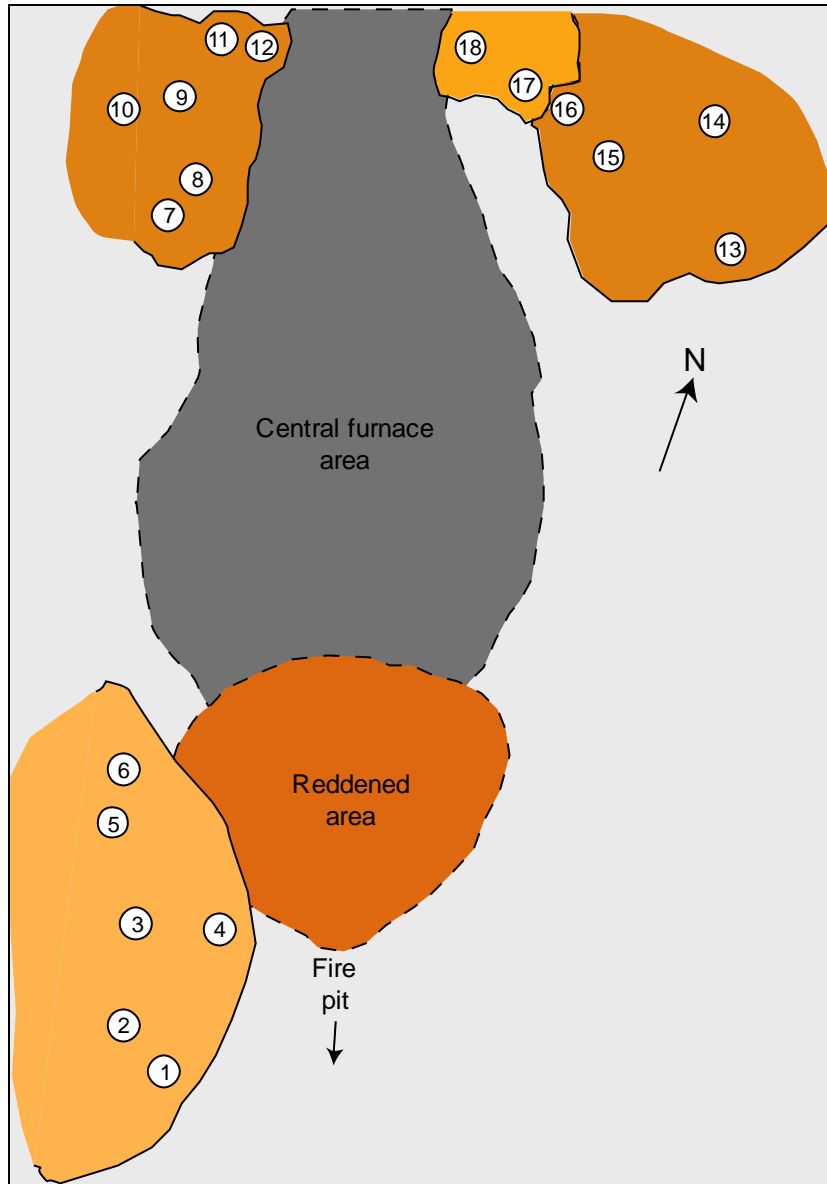
*Figure 5: Sketch plan showing distribution of samples on fired clay areas at site 15a (not to scale).*

*Site 15a*

These heated clay remains were again in relatively good condition and there was evidence that this furnace was contained within a ditched enclosure. Approximate sample locations are depicted in Figure 5 and sample measurements are recorded in Tables 11 and 12. Figure 24 depicts the distribution of sample TRM directions before and after partial demagnetisation. Figures 25 illustrates the results of pilot demagnetisation on sample 15ABP09 (pilot demagnetisation was also carried out on samples 13ABP02 and 18). The magnetisation directions of these samples were stable with some viscous realignment in domains with coercivities below 10mT. Samples 15ABP02 and 04 were very small samples and were rejected as being unreliable. Samples 15ABP16-18 also had anomalous magnetisation directions. All three came from the same raised area of hardened clay near the edge of the excavated section.  It was concluded that, being raised, this area was likely to have been disturbed by ploughing, or by the mechanical excavator used to expose the feature and these

samples were also rejected. Figure 26 shows the comparison of the calculated mean TRM vector with the UK archaeomagnetic calibration curve.
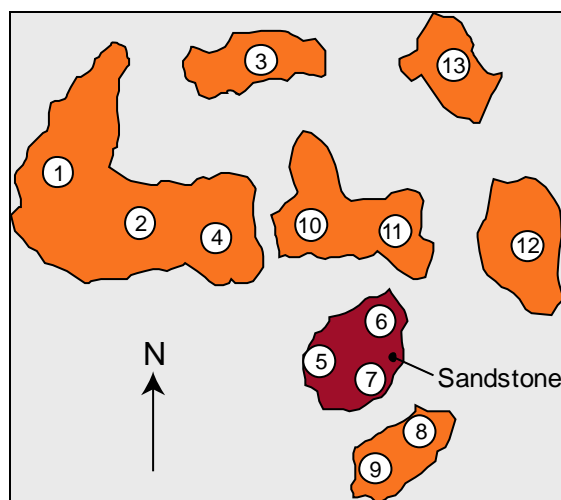


*Figure 6: Sketch plan showing distribution of samples on fired clay areas at site 15b (not to scale).*

*Site 15b*

These remains were located some 30 metres from site 15a on the crest of a slope. They were particularly badly damaged by ploughing because of this positioning. Little obviously fired material was apparent and all the samples were drawn from a single small patch of clay and sandstone some 40cm in diameter. Approximate sample locations are depicted in Figure 6 and sample measurements are recorded in Table 13. Figure 27 depicts the distribution of sample NRM directions. The sample NRM directions are extremely widely scattered and it was concluded that the sampled area was the remains of a pit of redeposited material. Thus no directional archaeomagnetic dating of this feature is possible.

## Conclusions

Archaeomagnetic analysis of the remains of a further six glass making furnaces from Bagot's Park has successfully inferred date ranges for five of them. The sixth, site 15b, was badly damaged by ploughing and it was difficult to find undisturbed, well-fired material. It would appear that the sampled area had been redeposited or heavily disturbed since the last firing of the furnace. Of the five furnaces for which dates could be obtained, only site 6b produced a disappointingly broad date range. This was to be expected as the nearby site 6a, sampled in 2000, also showed a high degree of scattering of sample TRM directions. These sites are low-lying and poorly drained. Thus it is possible that soil saturation during wet periods has led both to dissolution of the iron minerals carrying the magnetic remanence and softened the areas of baked clay making them more susceptible to disturbance by ploughing.

The date ranges derived for the last firings of the five dated furnaces are summarised below and compared with the preliminary archaeological assessments of the sites.

*Site 6b*

**1445 to 1500 AD at the 63% confidence level.**
**1410 to 1520 AD at the 95% confidence level.**

It was assumed, due to their close proximity, that this site was contemporary with 6a. The site has been fieldwalked, and there was little pottery. The absence of brick might suggest a date before 1500, by comparison with other sites. The archaeomagnetic date ranges for both 6a and 6b were broad with a fair degree of overlap. Hence, the hypothesis that sites 6a and 6b were in fact contemporary was tested, by assessing the probability that the mean TRM vectors measured for each were both estimates of the same underlying direction. The test of McFadden and Lowes (1981) indicated a probability of only 4.3% that the two mean TRM directions, given their respective precisions, are in fact both estimates of the same direction. Hence, the hypothesis that 6a and 6b are contemporary can be rejected at the 95% confidence level.

*Site 13a*

**1395 to 1445 AD at the 63% confidence level.**
**1380 to 1480 AD at the 95% confidence level.**

*Site 13b*

**1380 to 1400 AD at the 63% confidence level.**
**1370 to 1415 AD at the 95% confidence level.**

These sites have not yet been fieldwalked, but the general absence of brick on both sites, the lack of glass and the low level of finds all point to an earlier, medieval date. The archaeomagnetic dates suggest that the furnaces might have been used consecutively, 13b being the earliest.

*Site 13c*

**1530 to 1550 AD at the 63% confidence level.**
**1525 to 1565 AD at the 95% confidence level.**

For the same reasons as 13a and b, an early date might be expected. The site has not been fieldwalked, but glasspot found during the excavation is not similar to that found at Wolseley (a mid-sixteenth century furnace) and so the two would not be expected to be contemporary. Hence, the archaeomagnetic date is surprising, the more so due to the proximity of this site to sites 13a and b, which appear date from a century earlier.

*Site 15a*

**1280 to 1305 AD at the 63% confidence level.**
**1270 to 1320 AD at the 95% confidence level.**

This site was fieldwalked in 1997 and a lot of pottery was found, thought to be associated with the occupation of a dwelling on the site whose presence is indicated by spreads of brick and tile. The assemblage was assessed, and consisted of Cistercian Wares, Midlands purple

fabrics, some yellow wares and a few fragments of German stoneware but with a small amount of earlier material. In addition, the lack of good quality glass suggested that the site was not associated with the French immigrant glassmakers who were active in Staffordshire from about 1580, all of which seem to indicate a sixteenth century date and probably one in the earlier part of the century (Welch, 1997). The much earlier date implied by the TRM results must suggest that the dwelling and its associated pottery are not related to each other. Whether the dwelling is associated with a later phase of glassmaking activity represented by furnace 15b remains to be determined.

On the magnetometer survey plot, furnace 15a was surrounded by a rectangular anomaly, which is very clearly associated with it and which on excavation proved to be a ditch. Sections were cut through the ditch and some pottery recovered. Debbie Ford examined the few fragments and identified them as iron rich sandy utilitarian ware (definition in Ford 1995), and suggested a date between the eleventh and the fourteenth centuries, thus supporting the TRM date.

It is instructive to note that, had fieldwalking not taken place, a 'traditional' excavation, concentrating on 15a and its surrounding feature and involving the initial removal of topsoil, excavation of features and supported by a TRM date would have correctly identified a medieval phase of glassmaking. However, it would not have identified a sixteenth century phase of occupation at all.

*General discussion*

Archaeomagnetic dates have now been obtained for twelve of the glassmaking furnaces at Bagot's Park. Eleven of these have been excavated and dated by the authors during 2000-2001. The other date is that obtained by Aitken and Hawley from Crossley's excavation of the then relatively well preserved furnace at site 4 (Crossley 1967, p81-3). Their mean TRM has been recalibrated using the more recent calibration data of Clark, Tarling and Noel (1988) so that it can be compared directly with the other archaeomagnetic dates, giving date ranges of:

**1530 to 1540 AD at the 63% confidence level.**
**1525 to 1545 AD at the 95% confidence level.**

All twelve date ranges have been plotted in Figure 7a and, looking at the spread of dates, a pattern begins to emerge. The greater number fall after 1400 (beginning with 13b), with a steady increase into the sixteenth century. This pattern is emphasised if site 11a (which cannot be dated) is included, since it is known from the associated finds to date from the period 1583-1615, and is unlikely to be dramatically altered by the dating of the remaining sites (17 and 18). Site 16 is also undated, but finds there also point to a later date. Two sites fall earlier, 11b and 15a. The TRM date of 11b is imprecise, with two possible ranges, the earliest of which falls in the thirteenth century. However, this earlier date range is supported by ceramic evidence. 15a has a precise date, strongly supported by ceramic evidence, which places it in use somewhere around 1300. This leaves something of a gap in the fourteenth century, filled by site 6a alone, although this is based on an imprecise TRM date.

Figure 7b illustrates this pattern in a quantitative way. It shows a histogram of the number of furnaces that were last used in each 50-year period between 1250 and 1600, based on the archaeomagnetic evidence. These sums were calculated by considering each 50 year time span in turn and adding the fraction of each furnace's 63% date range that overlapped the

11

span to its total. It should be borne in mind that the archaeomagnetic dates estimate the last firing of each furnace, hence there will be some time lag inherent in the trends indicated in the histogram. Nevertheless, Figure 7b suggests that glassmaking furnaces first appear on the site in the latter half of the 13th century AD with 2 furnaces in operation. There then appears to be a hiatus until the later part of the 14th century when two more furnaces are last used. Glassmaking then seems to continue at about the same level until the turn of the 16th century AD when it peaks, with 4.5 furnaces being last used between 1500 and 1550. Further research will be required to ascertain whether this trough and peak in production can be correlated with variability in demand for glass. As yet no furnaces have been dated later than 1550 AD, although documentary evidence attests to the continuation of glassmaking at Bagot's Park until the early 17th century.

One further factor that emerges from the archaeomagnetic analysis, is that furnaces in close proximity to one another do not necessarily date from the same period. This is most clearly demonstrated with the results from furnaces 13a and b, which predate 13c by a century. The same appears to be true of sites 6a and b but the distinction is less certain owing to the poor precision of the mean TRMs obtained. Furthermore, furnace 11b appears to be early in date whilst artefactual evidence suggests that 11a dates from the 1580-1615 period. Furnace 15a also appears to predate much of the archaeological evidence found in close proximity to it. The latter may be associated with furnace 15b but it will not be possible to confirm this conjecture unless it is possible to resample 15b and obtain an archaeomagnetic date. However, it appears possible that spatial proximity does not necessarily indicate a direct succession of furnaces constructed by the same artisans. Instead glassmakers might have chosen to use sites close to much earlier furnaces, perhaps due to proximity of resources, or to exploit the earlier furnace remains as a source of building materials to construct their own furnace.

P. Linford                                                        Date of report: 15/11/2001
Archaeometry Branch,
Centre for Archaeology, English Heritage.

C. Welch
Principal Archaeological Officer
Development Services Department
Staffordshire County Council
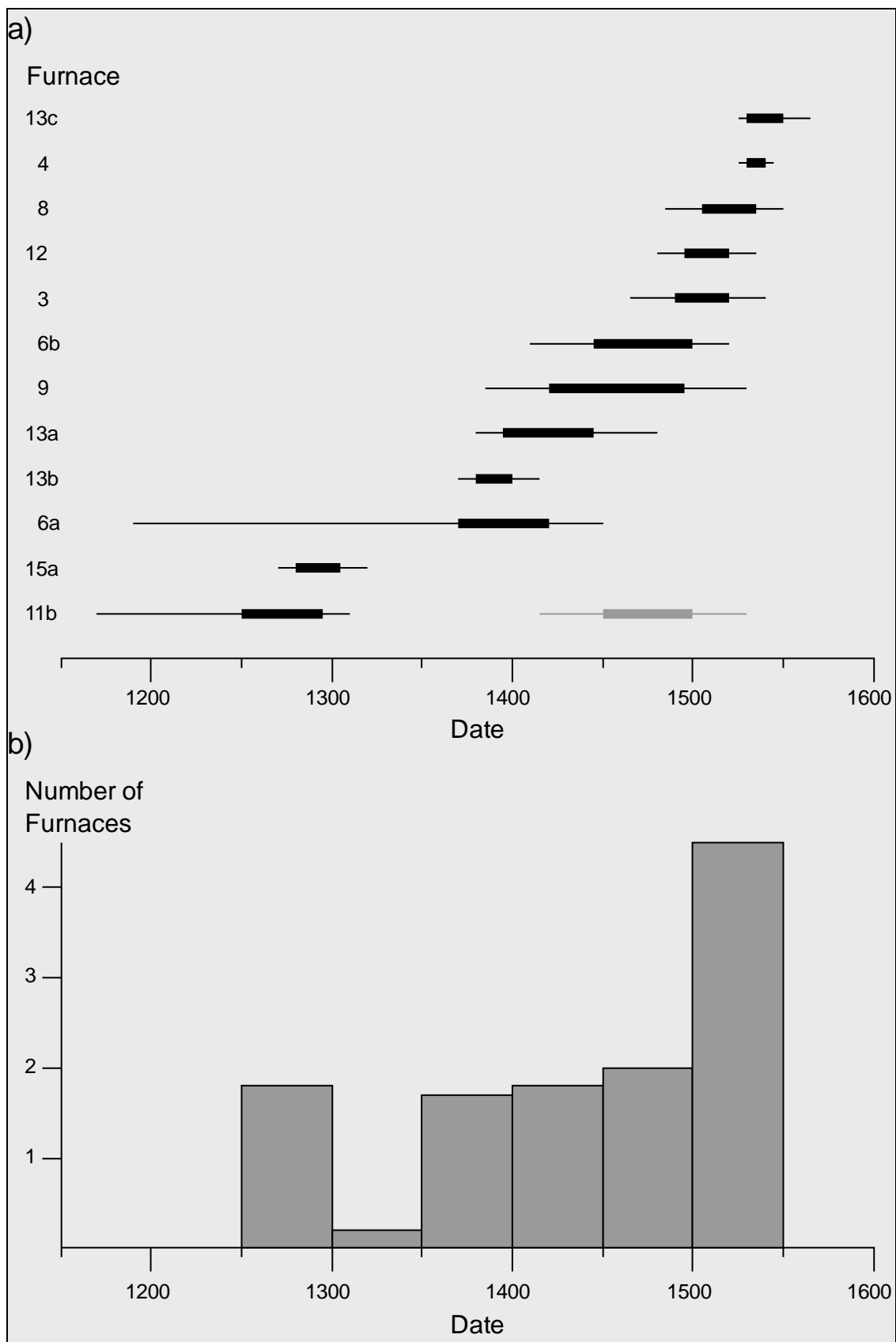
*Figure 7: a) Archaeomagnetic date ranges of features from Bagot's Park. Thin lines represent 95% confidence intervals, thick lines represent 63% confidence intervals. Note the second possible date range for 11b shown in grey. b) Number of furnaces last fired in each 50-year period between 1250 and 1600 AD.*

**Archaeomagnetic Date Summary**

| | |
|---|---|
| Archaeomagnetic ID: | **6BBP** |
| Feature: | **Bagot's Park, site 6b** |
| Location: | **Longitude 1.9$^o$W, Latitude 52.8$^o$N** |
| Number of Samples (taken/used in mean): | **17/11** |
| AF Demagnetisation Applied: | **5mT** |
| Distortion Correction Applied: | **+2.4 $^o$** |
| Declination (at Meriden): | **6.8$^o$ (6.8$^o$)** |
| Inclination (at Meriden): | **61.0$^o$ (60.7 $^o$)** |
| Alpha-95: | **3.8$^o$** |
| k: | **145.5** |
| Date range (63% confidence): | **1445 AD to 1500 AD** |
| Date range (95% confidence): | **1410 AD to 1520 AD** |

| | |
|---|---|
| Archaeomagnetic ID: | **13ABP** |
| Feature: | **Bagot's Park, site 13a** |
| Location: | **Longitude 1.9$^o$W, Latitude 52.8$^o$N** |
| Number of Samples (taken/used in mean): | **16/12** |
| AF Demagnetisation Applied: | **5mT** |
| Distortion Correction Applied: | **+2.4 $^o$** |
| Declination (at Meriden): | **4.8$^o$ (4.8$^o$)** |
| Inclination (at Meriden): | **57.1$^o$ (56.8 $^o$)** |
| Alpha-95: | **3.9$^o$** |
| k: | **126.7** |
| Date range (63% confidence): | **1395 AD to 1445 AD** |
| Date range (95% confidence): | **1380 AD to 1480 AD** |

| | |
|---|---|
| Archaeomagnetic ID: | **13BBP** |
| Feature: | **Bagot's Park, site 13b** |
| Location: | **Longitude 1.9$^o$W, Latitude 52.8$^o$N** |
| Number of Samples (taken/used in mean): | **18/17** |
| AF Demagnetisation Applied: | **10 or 50mT** |
| Distortion Correction Applied: | **+2.4 $^o$** |
| Declination (at Meriden): | **-1.1$^o$ (-1.0$^o$)** |
| Inclination (at Meriden): | **56.7$^o$ (56.3 $^o$)** |
| Alpha-95: | **2.4$^o$** |
| k: | **230.6** |
| Date range (63% confidence): | **1380 AD to 1400 AD** |
| Date range (95% confidence): | **1370 AD to 1415 AD** |

Archaeomagnetic ID:                                   **13CBP**
Feature:                                              **Bagot's Park, site 13c**
Location:                                             **Longitude 1.9$^o$W, Latitude 52.8$^o$N**
Number of Samples (taken/used in mean):               **20/17**
AF Demagnetisation Applied:                           **10 or 50mT**
Distortion Correction Applied:                        **+2.4$^o$**
Declination (at Meriden):                             **10.2$^o$ (10.1$^o$)**
Inclination (at Meriden):                             **67.2$^o$ (67.0$^o$)**
Alpha-95:                                             **1.9$^o$**
k:                                                    **353.1**
Date range (63% confidence):                          **1530 AD to 1550 AD**
Date range (95% confidence):                          **1525 AD to 1565 AD**

Archaeomagnetic ID:                                   **15ABP**
Feature:                                              **Bagot's Park, site 15a**
Location:                                             **Longitude 1.9$^o$W, Latitude 52.8$^o$N**
Number of Samples (taken/used in mean):               **18/13**
AF Demagnetisation Applied:                           **10mT**
Distortion Correction Applied:                        **+2.4$^o$**
Declination (at Meriden):                             **2.8$^o$ (2.8$^o$)**
Inclination (at Meriden):                             **61.3$^o$ (61.0$^o$)**
Alpha-95:                                             **2.2$^o$**
k:                                                    **350.3**
Date range (63% confidence):                          **1280 AD to 1305 AD**
Date range (95% confidence):                          **1270 AD to 1320 AD**

Archaeomagnetic ID:                                   **15BBP**
Feature:                                              **Bagot's Park, site 15b**
Location:                                             **Longitude 1.9$^o$W, Latitude 52.8$^o$N**
Number of Samples (taken/used in mean):               **13/-**
AF Demagnetisation Applied:                           **-**
Distortion Correction Applied:                        **-**
Declination (at Meriden):                             **-**
Inclination (at Meriden):                             **-**
Alpha-95:                                             **-**
k:                                                    **-**
Date range (63% confidence):                          **undatable**
Date range (95% confidence):                          **undatable**

|  |  | NRM Measurements | | | | After Partial Demagnetisation | | | |
|---|---|---|---|---|---|---|---|---|---|
| Sample | Material | Dec° | Inc° | J(mAm⁻¹) | AF(mT) | Dec° | Inc° | J(mAm⁻¹) | R |
| 6BBP01 | Clay | -32.5 | 49.2 | 44.0 | 5.0 | -35.2 | 48.3 | 38.1 | R |
| 6BBP02 | Clay | -30.0 | 55.2 | 1281.7 | 5.0 | -38.1 | 55.4 | 1010.2 | R |
| 6BBP03 | Clay | 19.1 | 65.5 | 402.0 | 5.0 | 7.7 | 64.2 | 338.3 | |
| 6BBP04 | Clay | -1.3 | 45.6 | 1290.5 | 5.0 | -3.1 | 42.8 | 1096.6 | R |
| 6BBP05 | Clay | -7.1 | 66.1 | 311.6 | 5.0 | -14.4 | 67.9 | 267.5 | R |
| 6BBP06 | Clay | 18.1 | 57.3 | 849.6 | 5.0 | 16.9 | 55.0 | 708.4 | |
| 6BBP07 | Clay | -12.9 | 57.8 | 449.8 | 5.0 | -10.8 | 56.1 | 393.5 | |
| 6BBP08 | Clay | 10.8 | 53.2 | 746.9 | 5.0 | 14.4 | 50.8 | 673.5 | |
| 6BBP09 | Clay | -71.5 | 80.7 | 493.8 | 5.0 | -69.1 | 82.3 | 460.0 | R |
| 6BBP10 | Clay | 7.3 | 66.7 | 592.6 | 5.0 | 10.2 | 64.5 | 497.7 | |
| 6BBP11 | Clay | -18.7 | 70.7 | 106.6 | 5.0 | -7.9 | 59.2 | 87.5 | |
| 6BBP12 | Clay | 12.3 | 61.2 | 292.5 | 5.0 | 7.6 | 59.2 | 237.4 | |
| 6BBP13 | Clay | 11.1 | 63.5 | 431.5 | 5.0 | 8.3 | 58.6 | 355.9 | |
| 6BBP14 | Clay | 12.6 | 53.0 | 1507.9 | 5.0 | 16.5 | 51.1 | 1380.9 | |
| 6BBP15 | Clay | 7.2 | 58.8 | 1283.3 | 5.0 | 6.9 | 58.2 | 1181.0 | |
| 6BBP16 | Clay | -1.0 | 66.7 | 742.5 | 5.0 | -0.1 | 64.8 | 664.2 | |
| 6BBP17 | Clay | -28.9 | 78.5 | 730.3 | 5.0 | -23.7 | 78.6 | 627.9 | R |

*Table 2: Sample NRM measurements and measurements after partial AF demagnetisation for feature 6BBP. J = magnitude of magnetisation vector; AF = peak alternating field strength of demagnetising field; R = sample rejected from mean calculation.*

|  | 6BBP02 | | | 6BBP09 | | | 6BBP13 | | |
|---|---|---|---|---|---|---|---|---|---|
| AF(mT) | Dec° | Inc° | J(mAm⁻¹) | Dec° | Inc° | J(mAm⁻¹) | Dec° | Inc° | J(mAm⁻¹) |
| 0.0 | -45.3 | 59.8 | 1267.9 | -71.5 | 80.7 | 493.8 | 7.1 | 61.8 | 444.6 |
| 2.5 | -41.4 | 57.3 | 1158.7 | -64.8 | 82.5 | 491.4 | 8.0 | 59.4 | 408.7 |
| 5.0 | -38.1 | 55.4 | 1010.2 | -69.1 | 82.3 | 460.0 | 8.3 | 58.6 | 355.9 |
| 10.0 | -35.1 | 53.6 | 651.9 | -64.8 | 82.9 | 375.2 | 10.3 | 55.9 | 234.8 |
| 15.0 | -32.7 | 52.5 | 391.0 | -61.0 | 83.4 | 271.1 | 10.5 | 53.1 | 123.3 |
| 20.0 | -33.1 | 53.5 | 252.4 | -50.9 | 82.5 | 176.4 | 9.6 | 50.9 | 69.8 |
| 30.0 | -31.1 | 50.5 | 169.2 | -55.6 | 78.7 | 84.9 | 8.3 | 45.5 | 35.9 |
| 50.0 | -33.4 | 55.4 | 117.0 | -46.4 | 71.8 | 48.1 | 6.8 | 40.0 | 21.1 |

*Table 3: Incremental partial demagnetisation measurements for samples 6BBP02, 6BBP09 and 6BBP13.*

| | | NRM Measurements | | | After Partial Demagnetisation | | | |
|---|---|---|---|---|---|---|---|---|---|
| Sample | Material | Dec° | Inc° | J(mAm⁻¹) | AF(mT) | Dec° | Inc° | J(mAm⁻¹) | R |
| 13ABP01 | Clay | 10.0 | 54.7 | 4815.3 | 5.0 | 12.1 | 54.7 | 4476.6 | |
| 13ABP02 | Clay | 16.1 | 59.7 | 521.8 | 5.0 | 17.2 | 60.5 | 437.7 | |
| 13ABP03 | Clay | 12.8 | 55.4 | 2259.2 | 5.0 | 12.0 | 55.2 | 1979.6 | |
| 13ABP04 | Clay | 10.6 | 46.6 | 7177.0 | 5.0 | 11.3 | 46.0 | 6618.7 | |
| 13ABP05 | Clay | 11.0 | 56.1 | 3207.0 | 5.0 | 5.6 | 54.0 | 2930.3 | |
| 13ABP06 | Clay | 1.1 | 66.6 | 936.3 | 5.0 | 1.5 | 65.7 | 889.8 | |
| 13ABP07 | Clay | 19.4 | 58.5 | 909.9 | 5.0 | 18.6 | 55.9 | 842.0 | |
| 13ABP08 | Clay | 111.0 | 63.3 | 100.8 | - | - | - | - | R |
| 13ABP09 | Clay | 174.2 | 18.7 | 108.1 | - | - | - | - | R |
| 13ABP10 | Clay | -27.7 | 42.9 | 2026.6 | - | - | - | - | R |
| 13ABP11 | Clay | -0.9 | 54.7 | 1127.8 | 5.0 | 1.7 | 54.4 | 1044.4 | |
| 13ABP12 | Clay | -120.4 | -2.9 | 182.7 | - | - | - | - | R |
| 13ABP13 | Clay | 5.4 | 54.1 | 7404.5 | 5.0 | -0.7 | 53.0 | 7236.6 | |
| 13ABP14 | Clay | -7.1 | 57.1 | 579.5 | 5.0 | -9.2 | 52.4 | 513.2 | |
| 13ABP15 | Clay | -1.4 | 51.9 | 559.8 | 5.0 | 0.3 | 51.2 | 545.0 | |
| 13ABP16 | Clay | -7.9 | 49.3 | 475.0 | 5.0 | -9.6 | 49.4 | 430.6 | |

*Table 4: Sample NRM measurements and measurements after partial AF demagnetisation for feature 13ABP. J = magnitude of magnetisation vector; AF = peak alternating field strength of demagnetising field; R = sample rejected from mean calculation.*

| | 13ABP04 | | | 13ABP06 | | | 13ABP13 | | |
|---|---|---|---|---|---|---|---|---|---|
| AF(mT) | Dec° | Inc° | J(mAm⁻¹) | Dec° | Inc° | J(mAm⁻¹) | Dec° | Inc° | J(mAm⁻¹) |
| 0.0 | 11.1 | 49.0 | 7224.8 | -1.5 | 67.7 | 962.0 | -3.3 | 54.1 | 8056.6 |
| 2.5 | 11.3 | 46.7 | 7210.7 | 0.7 | 67.1 | 933.6 | -1.8 | 53.5 | 7706.3 |
| 5.0 | 11.3 | 46.0 | 6618.7 | 1.5 | 65.7 | 889.8 | -0.7 | 53.0 | 7236.6 |
| 10.0 | 11.2 | 44.3 | 4670.6 | 1.9 | 66.2 | 731.4 | 0.9 | 52.5 | 5416.8 |
| 15.0 | 11.3 | 44.7 | 3076.9 | 2.2 | 65.6 | 518.3 | -0.1 | 52.1 | 3628.7 |
| 20.0 | 11.8 | 45.1 | 2197.7 | 2.0 | 65.2 | 355.9 | 0.0 | 52.2 | 2158.4 |
| 30.0 | 11.8 | 44.3 | 1637.2 | 0.2 | 63.7 | 188.4 | 0.8 | 49.2 | 968.7 |
| 50.0 | 13.5 | 44.8 | 1297.0 | 0.2 | 68.3 | 115.9 | 1.1 | 52.8 | 503.9 |
| 75.0 | 12.1 | 44.7 | 1148.0 | -1.4 | 64.0 | 104.7 | 19.1 | 50.9 | 256.3 |
| 100.0 | - | - | - | -0.7 | 64.4 | 97.1 | - | - | - |

*Table 5: Incremental partial demagnetisation measurements for samples 13ABP04, 13ABP06 and 13ABP13.*

| | | NRM Measurements | | | After | Partial | Demagnetisation | | |
|---|---|---|---|---|---|---|---|---|---|
| Sample | Material | Dec° | Inc° | J (mAm$^{-1}$) | AF (mT) | Dec° | Inc° | J (mAm$^{-1}$) | R |
| 13BBP01 | Clay | 18.5 | 48.9 | 285.3 | 50.0 | 15.1 | 47.4 | 153.0 | R |
| 13BBP02 | Clay | 0.9 | 60.0 | 1081.3 | 10.0 | 1.1 | 59.7 | 1011.0 | |
| 13BBP03 | Clay | 4.0 | 59.5 | 2614.1 | 10.0 | 4.1 | 59.6 | 2509.5 | |
| 13BBP04 | Clay | 1.3 | 55.8 | 2617.3 | 10.0 | 1.1 | 55.2 | 2545.7 | |
| 13BBP05 | Clay | 5.0 | 59.2 | 17912.3 | 10.0 | 4.5 | 58.6 | 15592.7 | |
| 13BBP06 | Clay | 4.2 | 55.4 | 13502.6 | 10.0 | 3.6 | 54.3 | 12130.6 | |
| 13BBP07 | Clay | 4.9 | 56.2 | 7751.0 | 10.0 | 4.8 | 55.6 | 7291.0 | |
| 13BBP08 | Clay | -0.5 | 57.1 | 1435.8 | 10.0 | -1.7 | 57.2 | 1301.5 | |
| 13BBP09 | Clay | -1.0 | 54.7 | 2748.0 | 10.0 | -0.5 | 54.8 | 2474.5 | |
| 13BBP10 | Clay | -15.0 | 56.7 | 1831.3 | 10.0 | -13.9 | 57.1 | 1766.3 | |
| 13BBP11 | Clay | 2.4 | 58.9 | 1169.6 | 10.0 | 3.4 | 57.9 | 1079.3 | |
| 13BBP12 | Clay | -7.5 | 59.5 | 9543.8 | 10.0 | -7.6 | 58.3 | 7893.8 | |
| 13BBP13 | Clay | -3.7 | 50.6 | 381.3 | 10.0 | -3.3 | 51.5 | 351.7 | |
| 13BBP14 | Clay | -1.9 | 51.7 | 5263.5 | 10.0 | -1.9 | 49.7 | 2669.4 | |
| 13BBP15 | Clay | 1.8 | 51.1 | 1338.7 | 10.0 | 1.2 | 50.6 | 922.1 | |
| 13BBP16 | Clay | -4.6 | 47.5 | 5063.3 | 10.0 | -5.6 | 46.2 | 4098.3 | |
| 13BBP17 | Clay | -0.5 | 44.0 | 1059.9 | 10.0 | -0.9 | 44.4 | 991.4 | |
| 13BBP18 | Clay | -6.3 | 52.1 | 4843.4 | 10.0 | -5.5 | 50.9 | 4347.0 | |

*Table 6: Sample NRM measurements and measurements after partial AF demagnetisation for feature 13BBP. J = magnitude of magnetisation vector; AF = peak alternating field strength of demagnetising field; R = sample rejected from mean calculation.*

| | 13BBP01 | | | 13BBP08 | | |
|---|---|---|---|---|---|---|
| AF (mT) | Dec° | Inc° | J (mAm$^{-1}$) | Dec° | Inc° | J (mAm$^{-1}$) |
| 0.0 | 19.3 | 47.5 | 284.8 | 0.3 | 58.0 | 1429.9 |
| 2.5 | 18.0 | 46.8 | 282.9 | -0.2 | 57.7 | 1426.3 |
| 5.0 | 18.3 | 47.1 | 281.3 | 0.4 | 57.8 | 1408.7 |
| 10.0 | 18.0 | 46.5 | 274.5 | -1.7 | 57.2 | 1301.5 |
| 15.0 | 17.3 | 46.2 | 263.4 | -0.7 | 57.0 | 1080.0 |
| 20.0 | 17.1 | 46.7 | 249.2 | -1.7 | 56.0 | 790.5 |
| 30.0 | 15.1 | 46.7 | 215.7 | -0.5 | 54.5 | 319.1 |
| 50.0 | 15.1 | 47.4 | 153.0 | 1.4 | 53.5 | 71.6 |
| 75.0 | 15.5 | 46.4 | 97.8 | -11.7 | 55.3 | 49.0 |
| 100.0 | 15.9 | 46.6 | 64.9 | - | - | - |

*Table 7: Incremental partial demagnetisation measurements for samples 13BBP01 and 13BBP08.*

| | | NRM Measurements | | | | After | Partial | Demagnetisation | |
|---|---|---|---|---|---|---|---|---|---|
| Sample | Material | Dec° | Inc° | J(mAm⁻¹) | AF(mT) | Dec° | Inc° | J(mAm⁻¹) | R |
| 13CBP01 | Clay | 5.2 | 61.8 | 3062.1 | 10.0 | 4.8 | 61.7 | 2626.1 | |
| 13CBP02 | S'stone | 1.7 | 66.0 | 3104.3 | 10.0 | 4.4 | 66.5 | 2643.5 | |
| 13CBP03 | S'stone | 5.8 | 67.5 | 1130.3 | 10.0 | 3.9 | 67.4 | 949.0 | |
| 13CBP04 | Clay | 2.3 | 62.1 | 615.8 | 10.0 | 2.7 | 62.3 | 478.0 | |
| 13CBP05 | Clay | 91.7 | 37.2 | 185.8 | 10.0 | 90.5 | 30.8 | 124.2 | R |
| 13CBP06 | Clay | -26.5 | 82.0 | 27.8 | 10.0 | -45.5 | 79.8 | 16.7 | R |
| 13CBP07 | Clay | 6.5 | 65.5 | 566.2 | 10.0 | 7.8 | 65.7 | 373.2 | |
| 13CBP08 | Clay | 4.4 | 70.1 | 555.1 | 10.0 | 8.3 | 67.1 | 427.1 | |
| 13CBP09 | Glss Slg | 1.5 | 65.0 | 1588.8 | 10.0 | 4.6 | 65.7 | 1319.3 | |
| 13CBP10 | Glss Slg | -1.8 | 64.3 | 24.8 | 10.0 | 0.2 | 66.3 | 21.6 | |
| 13CBP11 | Glss Slg | -0.5 | 68.4 | 875.2 | 50.0 | 3.4 | 67.7 | 422.9 | |
| 13CBP12 | Glss Slg | 7.7 | 62.5 | 601.9 | 10.0 | 6.6 | 62.5 | 523.8 | |
| 13CBP13 | Clay | -173.2 | 77.7 | 1937.6 | 10.0 | -178.7 | 77.3 | 1359.5 | R |
| 13CBP14 | Clay | 35.8 | 64.7 | 4277.2 | 10.0 | 36.4 | 63.8 | 3115.3 | |
| 13CBP15 | Clay | 10.1 | 59.6 | 160.3 | 10.0 | 10.0 | 59.3 | 148.5 | |
| 13CBP16 | Clay | 17.7 | 63.8 | 34877.0 | 10.0 | 19.5 | 64.1 | 26980.4 | |
| 13CBP17 | Clay | 24.8 | 64.3 | 2721.1 | 10.0 | 23.4 | 63.7 | 1496.7 | |
| 13CBP18 | Clay | 20.4 | 65.1 | 3988.6 | 10.0 | 20.1 | 64.6 | 2705.3 | |
| 13CBP19 | Clay | 7.8 | 64.5 | 2641.7 | 10.0 | 7.8 | 64.2 | 2468.6 | |
| 13CBP20 | Clay | 5.5 | 65.3 | 1963.7 | 10.0 | 7.0 | 65.3 | 1838.9 | |

*Table 8: Sample NRM measurements and measurements after partial AF demagnetisation for feature 13CBP. J = magnitude of magnetisation vector; AF = peak alternating field strength of demagnetising field; R = sample rejected from mean calculation. S'stone = Sandstone, Glss Slg = Glass Slag.*

| | 13CBP02 | | | 13CBP05 | | | 13CBP08 | | |
|---|---|---|---|---|---|---|---|---|---|
| AF(mT) | Dec° | Inc° | J(mAm⁻¹) | Dec° | Inc° | J(mAm⁻¹) | Dec° | Inc° | J(mAm⁻¹) |
| 0.0 | 4.4 | 67.0 | 3155.0 | 90.6 | 39.0 | 195.2 | 8.9 | 68.7 | 576.3 |
| 2.5 | 4.2 | 66.4 | 3091.3 | 90.7 | 34.4 | 185.3 | 9.0 | 68.5 | 553.9 |
| 5.0 | 5.0 | 66.8 | 3004.9 | 90.5 | 32.2 | 169.1 | 9.2 | 68.5 | 521.4 |
| 10.0 | 4.4 | 66.5 | 2643.5 | 90.5 | 30.8 | 124.2 | 8.3 | 67.1 | 427.1 |
| 15.0 | 4.2 | 66.8 | 2123.6 | 89.0 | 30.3 | 86.5 | 7.8 | 67.4 | 329.5 |
| 20.0 | 3.3 | 66.5 | 1733.5 | 89.3 | 30.4 | 60.2 | 8.3 | 66.8 | 242.0 |
| 30.0 | 4.4 | 67.1 | 1217.3 | 91.6 | 26.2 | 34.4 | 9.2 | 67.3 | 138.4 |
| 50.0 | 3.4 | 66.4 | 765.2 | 101.0 | 26.7 | 19.6 | 18.5 | 68.9 | 67.1 |
| 75.0 | 2.7 | 66.5 | 578.0 | 96.6 | 23.4 | 16.0 | 23.6 | 67.1 | 48.4 |
| 100.0 | 3.3 | 67.4 | 517.0 | - | - | - | - | - | - |

*Table 9: Incremental partial demagnetisation measurements for samples 13CBP02, 13CBP05 and 13CBP08.*

| AF(mT) | 13CBP11 Dec° | Inc° | J(mAm⁻¹) | 13CBP12 Dec° | Inc° | J(mAm⁻¹) | 13CBP13 Dec° | Inc° | J(mAm⁻¹) |
|---|---|---|---|---|---|---|---|---|---|
| 0.0 | -0.3 | 68.7 | 881.6 | 6.7 | 62.3 | 600.3 | -177.3 | 79.0 | 1968.9 |
| 2.5 | 1.6 | 68.9 | 851.9 | 6.9 | 62.3 | 587.4 | -175.7 | 78.2 | 1896.3 |
| 5.0 | 1.7 | 68.1 | 829.6 | 7.2 | 62.3 | 568.6 | -175.5 | 77.8 | 1783.7 |
| 10.0 | 1.6 | 68.5 | 792.3 | 6.6 | 62.5 | 523.8 | -178.7 | 77.3 | 1359.5 |
| 15.0 | 2.2 | 68.3 | 750.0 | 7.3 | 62.3 | 483.6 | -179.1 | 77.5 | 798.1 |
| 20.0 | 1.7 | 67.8 | 699.0 | 7.4 | 62.1 | 451.6 | -171.6 | 77.9 | 365.8 |
| 30.0 | 1.8 | 68.3 | 598.6 | 7.1 | 62.8 | 413.1 | -156.3 | 78.6 | 108.2 |
| 50.0 | 3.4 | 67.7 | 422.9 | 8.3 | 61.9 | 364.5 | -72.0 | 78.8 | 31.0 |
| 75.0 | 3.8 | 66.4 | 315.6 | 6.9 | 62.9 | 347.2 | - | - | - |
| 100.0 | 3.8 | 66.7 | 259.8 | 6.9 | 62.1 | 337.5 | - | - | - |

*Table 10: Incremental partial demagnetisation measurements for samples 13CBP11, 13CBP12 and 13CBP13.*

| Sample | Material | NRM Measurements Dec° | Inc° | J(mAm⁻¹) | AF(mT) | After Partial Demagnetisation Dec° | Inc° | J(mAm⁻¹) | R |
|---|---|---|---|---|---|---|---|---|---|
| 15ABP01 | Clay | 9.2 | 55.3 | 1078.2 | 10.0 | 8.6 | 53.3 | 794.0 | |
| 15ABP02 | Clay | 50.2 | 61.8 | 1541.1 | 10.0 | 51.8 | 61.4 | 1184.4 | R |
| 15ABP03 | Clay | -0.7 | 54.1 | 2463.1 | 10.0 | -0.6 | 51.9 | 1565.8 | |
| 15ABP04 | Clay | 33.9 | 58.0 | 300.6 | 10.0 | 34.9 | 56.6 | 243.8 | R |
| 15ABP05 | Clay | 7.3 | 58.8 | 4059.8 | 10.0 | 6.1 | 57.8 | 3423.1 | |
| 15ABP06 | Clay | -7.8 | 65.4 | 455.9 | 10.0 | -7.8 | 64.5 | 370.6 | |
| 15ABP07 | Clay | -1.8 | 60.6 | 2236.2 | 10.0 | -1.5 | 60.6 | 2077.5 | |
| 15ABP08 | Clay | 4.7 | 58.1 | 2148.7 | 10.0 | 4.7 | 57.9 | 1991.9 | |
| 15ABP09 | Clay | 5.1 | 61.3 | 5287.0 | 10.0 | 2.8 | 60.9 | 4882.9 | |
| 15ABP10 | Clay | -3.2 | 59.2 | 2128.0 | 10.0 | -1.9 | 59.2 | 2001.0 | |
| 15ABP11 | Clay | 3.3 | 57.2 | 1430.6 | 10.0 | 4.6 | 58.9 | 1301.5 | |
| 15ABP12 | Clay | 5.7 | 56.3 | 3585.8 | 10.0 | 6.2 | 56.5 | 3389.4 | |
| 15ABP13 | Clay | -5.2 | 62.4 | 15376.0 | 10.0 | -5.5 | 61.9 | 12071.8 | |
| 15ABP14 | Clay | 8.6 | 60.5 | 6763.4 | 10.0 | 8.8 | 58.3 | 5359.6 | |
| 15ABP15 | Clay | 8.3 | 62.2 | 7730.2 | 10.0 | 8.1 | 62.2 | 7077.9 | |
| 15ABP16 | Clay | 57.2 | 33.6 | 454.4 | 10.0 | 57.5 | 32.4 | 437.7 | R |
| 15ABP17 | Clay | -22.5 | 67.2 | 829.9 | 10.0 | -21.8 | 66.7 | 778.4 | R |
| 15ABP18 | Clay | 36.2 | 47.9 | 2686.2 | 10.0 | 36.5 | 49.0 | 2492.0 | R |

*Table 11: Sample NRM measurements and measurements after partial AF demagnetisation for feature 15ABP. J = magnitude of magnetisation vector; AF = peak alternating field strength of demagnetising field; R = sample rejected from mean calculation.*

| AF(mT) | 15ABP02 | | | 15ABP09 | | | 15ABP18 | | |
|---|---|---|---|---|---|---|---|---|---|
| | Dec° | Inc° | J(mAm$^{-1}$) | Dec° | Inc° | J(mAm$^{-1}$) | Dec° | Inc° | J(mAm$^{-1}$) |
| 0.0 | 52.2 | 62.3 | 1589.5 | 3.0 | 61.3 | 5268.6 | 36.6 | 48.8 | 2679.2 |
| 2.5 | 52.0 | 62.2 | 1537.4 | 2.7 | 61.1 | 5218.2 | 36.8 | 48.8 | 2669.3 |
| 5.0 | 51.6 | 62.0 | 1445.6 | 3.5 | 61.1 | 5169.1 | 36.7 | 48.8 | 2623.3 |
| 10.0 | 51.8 | 61.4 | 1184.4 | 2.8 | 60.9 | 4882.9 | 36.5 | 49.0 | 2492.0 |
| 15.0 | 52.0 | 61.2 | 911.2 | 3.0 | 60.8 | 4365.0 | 36.8 | 49.3 | 2210.6 |
| 20.0 | 51.2 | 61.0 | 657.2 | 3.0 | 60.7 | 3702.2 | 38.1 | 49.5 | 1825.9 |
| 30.0 | 50.7 | 60.8 | 372.7 | 2.5 | 60.0 | 2110.6 | 37.3 | 47.9 | 982.6 |
| 50.0 | 50.8 | 59.7 | 226.9 | 0.7 | 59.3 | 716.5 | 38.9 | 46.9 | 387.3 |
| 75.0 | 50.3 | 58.1 | 187.7 | 0.2 | 57.3 | 489.0 | 39.8 | 46.8 | 277.7 |

*Table 12: Incremental partial demagnetisation measurements for samples 15ABP02, 15ABP09 and 15ABP18.*

| | NRM Measurements | | | |
|---|---|---|---|---|
| Sample | Material | Dec° | Inc° | J(mAm$^{-1}$) |
| 15BBP01 | Clay | -39.5 | 49.7 | 4454.6 |
| 15BBP02 | Clay | -37.6 | 8.3 | 742.6 |
| 15BBP03 | Clay | 136.3 | 3.1 | 647.5 |
| 15BBP04 | Clay | -18.2 | -9.8 | 246.7 |
| 15BBP05 | Sandstone | 71.7 | 21.5 | 33.6 |
| 15BBP06 | Sandstone | 77.2 | 24.6 | 761.6 |
| 15BBP07 | Sandstone | 79.2 | 21.5 | 21.6 |
| 15BBP08 | Clay | -113.5 | 45.8 | 6736.3 |
| 15BBP09 | Clay | -112.2 | 47.3 | 4136.7 |
| 15BBP10 | Clay | 29.4 | -47.7 | 6057.4 |
| 15BBP11 | Clay | 9.3 | -53.1 | 2317.1 |
| 15BBP12 | Clay | -67.3 | -12.7 | 19594.0 |
| 15BBP13 | Clay | 57.4 | -18.3 | 115.7 |

*Table 13: Sample NRM measurements for feature 15BBP. J = magnitude of magnetisation vector.*

**Appendix: Standard Procedures for Sampling and Measurement**

**1) Sampling**

One of three sampling techniques is employed depending on the consistency of the material (Clark, Tarling and Noel 1988):

a)      **Consolidated materials:** Rock and fired clay samples are collected by the disc method. Several small levelled plastic discs are glued to the feature, marked with an orientation line related to True North, then removed with a small piece of the material attached.

b)      **Unconsolidated materials:** Sediments are collected by the tube method. Small pillars of the material are carved out from a prepared platform, then encapsulated in levelled plastic tubes using plaster of Paris. The orientation line is then marked on top of the plaster.

c)      **Plastic materials:** Waterlogged clays and muds are sampled in a similar manner to method 1b) above; however, the levelled plastic tubes are pressed directly into the material to be sampled.

**2) Physical Analysis**

a)      Magnetic remanences are measured using a slow speed spinner fluxgate magnetometer (Molyneux et al. 1972; see also Tarling 1983, p84; Thompson and Oldfield 1986, p52).

b)      Partial demagnetisation is achieved using the alternating magnetic field method (As 1967; Creer 1959; see also Tarling 1983, p91; Thompson and Oldfield 1986, p59), to remove viscous magnetic components if necessary. Demagnetising fields are measured in milli-Tesla (mT), figures quoted being for the peak value of the field.

**3) Remanent Field Direction**

a)      The remanent field direction of a sample is expressed as two angles, declination (Dec) and inclination (Inc), both quoted in degrees. Declination represents the bearing of the field relative to true north, angles to the east being positive; inclination represents the angle of dip of this field.

b)      Aitken and Hawley (1971) have shown that the angle of inclination in measured samples is likely to be distorted owing to magnetic refraction. The phenomenon is not well understood but is known to depend on the position the samples occupied within the structure. The corrections recommended by Aitken and Hawley are applied, where appropriate, to measured inclinations, in keeping with the practise of Clark, Tarling and Noel (1988).

**c)**     Individual remanent field directions are combined to produce the mean remanent field direction using the statistical method developed by R. A. Fisher (1953). The quantity $\alpha_{95}$, "alpha-95", is quoted with mean field directions and is a measure of the precision of the determination (see Aitken 1990, p247). It is analogous to the standard error statistic for scalar quantities; hence the smaller its value, the better the precision of the date.

**d)**     For the purposes of comparison with standardised UK calibration data, remanent field directions are adjusted to the values they would have had if the feature had been located at Meriden, a standard reference point. The adjustment is done using the method suggested by Noel (Tarling 1983, p116).

## 4) Calibration

**a)**     Material less than 3000 years old is dated using the archaeomagnetic calibration curve compiled by Clark, Tarling and Noel (1988).

**b)**     Older material is dated using the lake sediment data compiled by Turner and Thompson (1982).

**c)**     Dates are normally given at the 63% and 95% confidence levels. However, the quality of the measurement and the estimated reliability of the calibration curve for the period in question are not taken into account, so this figure is only approximate. Owing to crossovers and contiguities in the curve, alternative dates are sometimes given. It may be possible to select the correct alternative using independent dating evidence.

**d)**     As the thermoremanent effect is reset at each heating, all dates for fired material refer to the final heating.

**e)**     Dates are prefixed by "cal", for consistency with the new convention for calibrated radiocarbon dates (Mook 1986).

**References**

Aitken, M. J. 1990. *Science-based Dating in Archaeology*. London: Longman.

Aitken, M. J. and H. N. Hawley 1971. Archaeomagnetism: evidence for magnetic refraction in kiln structures. *Archaeometry* **13**, 83-85.

As, J. A. 1967. The a.c. demagnetisation technique, in *Methods in Palaeomagnetism*, D. W. Collinson, K. M. Creer and S. K. Runcorn (eds). Amsterdam: Elsevier.

Clark, A. J., D. H. Tarling and M. Noel 1988. Developments in Archaeomagnetic Dating in Britain. *J. Arch. Sci.* **15**, 645-667.

Creer, K. M. 1959. A.C. demagnetisation of unstable Triassic Keuper Marls from S. W. England. *Geophys. J. R. Astr. Soc.* **2**, 261-275.

Crossley, D. W. 1967. Glassmaking in Bagot's Park Staffordshire, in the Sixteenth Century. *Post Medieval Archaeology* **1**, 44-83.

Fisher, R. A. 1953. Dispersion on a sphere. *Proc. R. Soc. London A* **217**, 295-305.

Ford, D. 1995. Medieval Pottery in Staffordshire, AD800-1600: A Review. *Staffordshire Archaeological Studies* **7**.

Linford, P. 2001. Bagot's Park, Abbots Bromley, Staffordshire. Archaeomagnetic Dating Report, 2001. Centre for Archaeology Report **17/2001**.

McFadden, P. L. and Lowes, F. J. 1981. The discrimination of mean directions drawn from Fisher distributions. *Geophys. J. R. Astr. Soc.* **67**, 19-33.

Molyneux, L., R. Thompson, F. Oldfield and M. E. McCallan 1972. Rapid measurement of the remanent magnetisation of long cores of sediment. *Nature* **237**, 42-43.

Mook, W. G. 1986. Recommendations/Resolutions Adopted by the Twelfth International Radiocarbon Conference. *Radiocarbon* **28**, M. Stuiver and S. Kra (eds), 799.

Tarling, D. H. 1983. *Palaeomagnetism*. London: Chapman and Hall.

Thompson, R. and F. Oldfield 1986. *Environmental Magnetism*. London: Allen and Unwin.

Turner, G. M. and R. Thompson 1982. Detransformation of the British geomagnetic secular variation record for Holocene times. *Geophys. J. R. Astr. Soc.* **70**, 789-792.

Welch, C. 1997. Glassmaking sites in Bagot's Park, Staffordshire. *West Midlands Archaeology* **40**, 8-12.

Welch, C. 1998. Bagot's Park, Abbots Bromley, Staffordshire. Investigation of ancient glassmaking sites. Interim report on work carried out in September-October 1998. *Unpublished report*.

*a)*
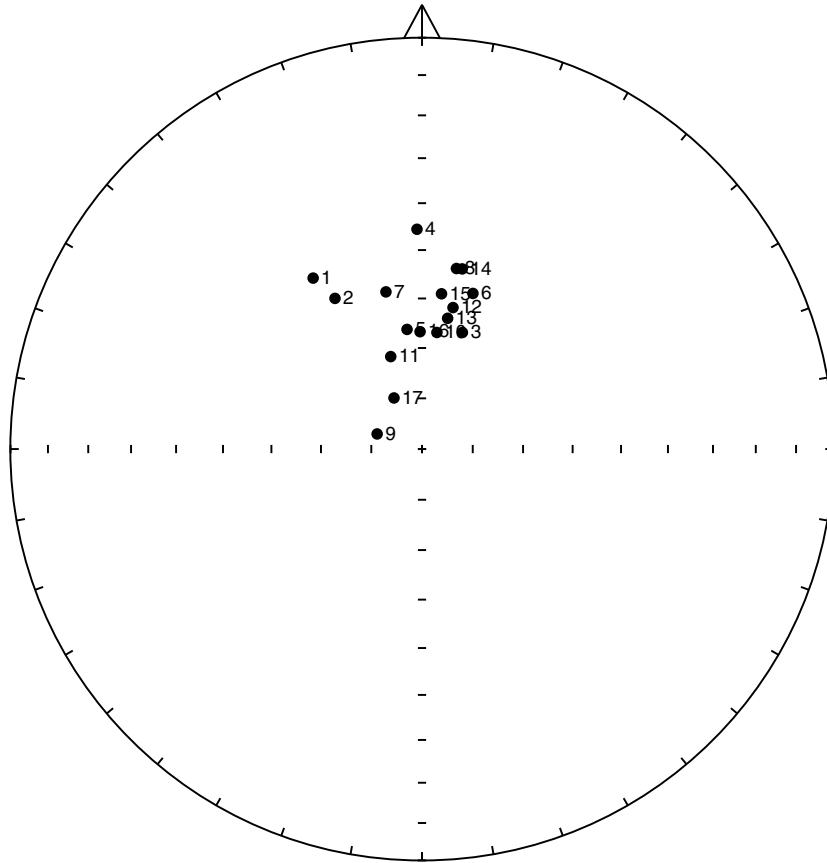


*b)*
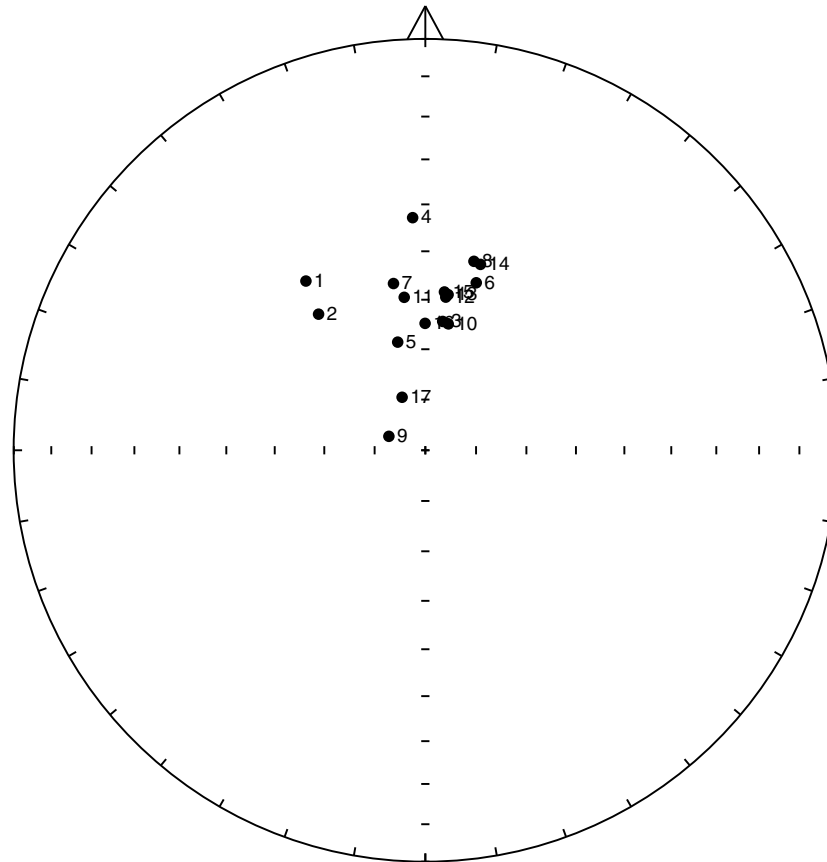


*Figure 8: a) Distribution of NRM directions of samples from feature 6BBP represented as an equal area stereogram. In this projection declination increases clockwise with zero being at 12 o'clock while inclination increases from zero at the equator to 90 degrees in the centre of the projection. Open circles represent negative inclinations. b) Distribution of thermoremanent directions of magnetisation of the same samples after partial AF demagnetisation to 5mT.*
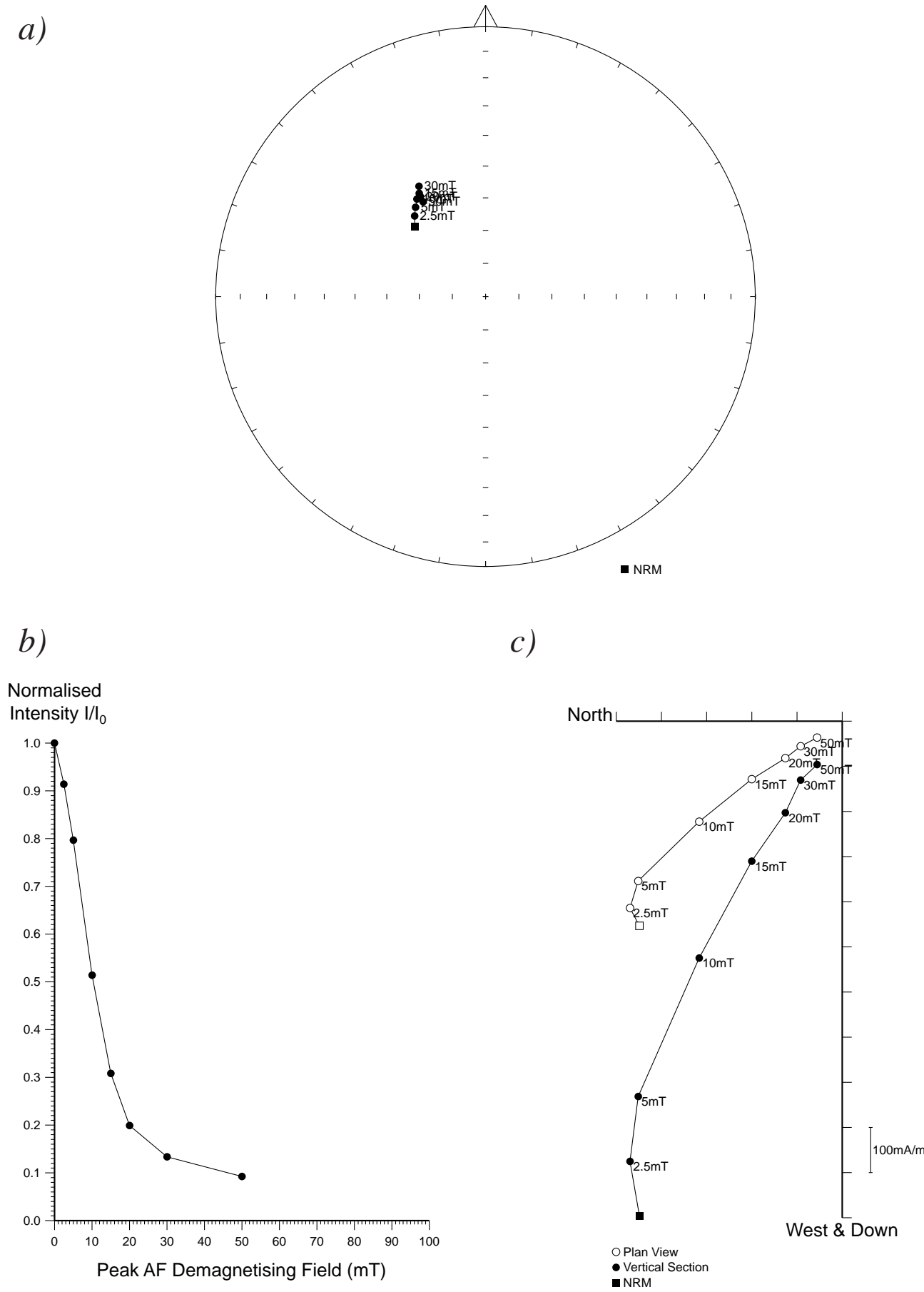
*Figure 9: Stepwise AF demagnetisation of sample 6BBP02. Diagram a) depicts the variation of the remanent direction as an equal area stereogram (declination increases clockwise, while inclination increases from zero at the equator to 90 degrees at the centre of the projection); b) shows the normalised change in remanence intensity as a function of the demagnetising field; c) shows the changes in both direction and intensity as a vector endpoint projection.*

26
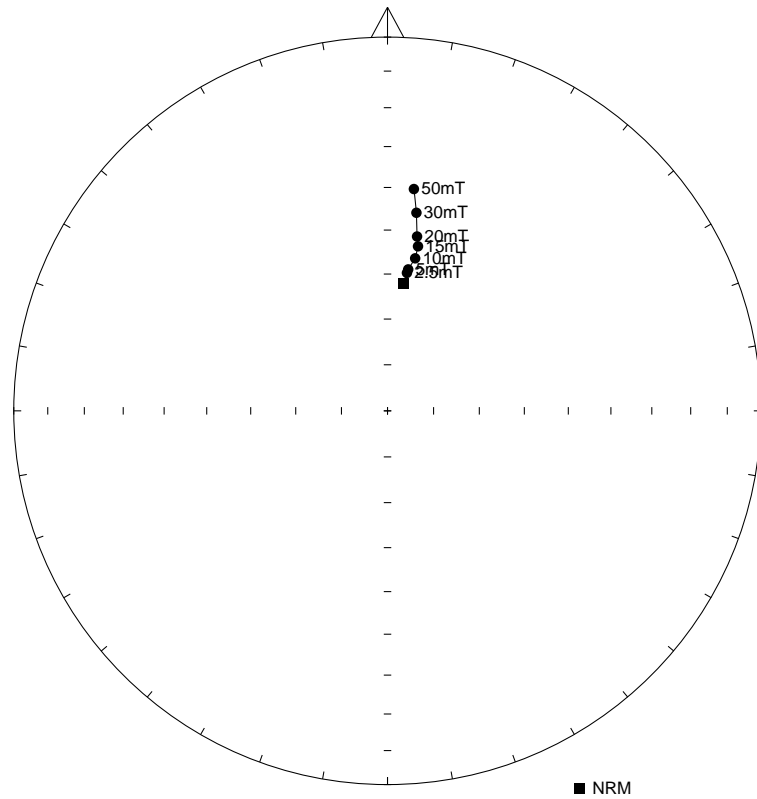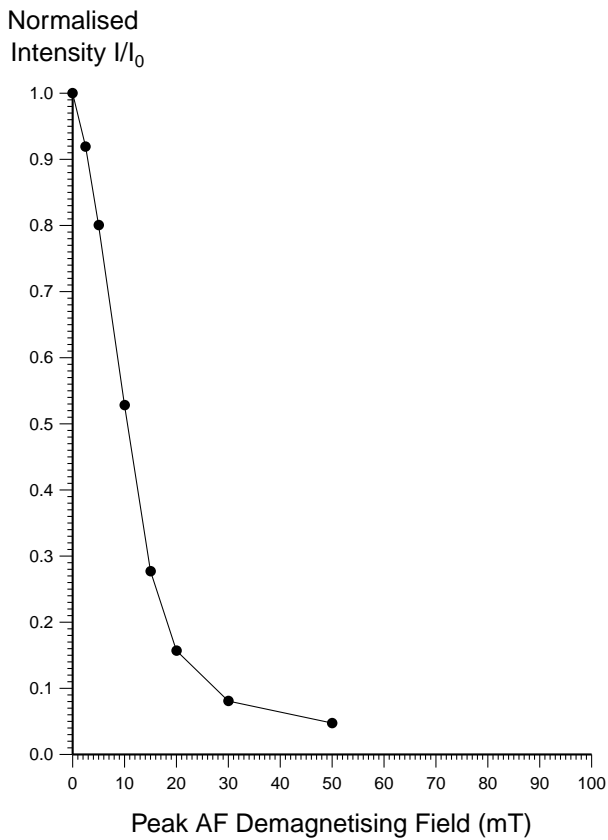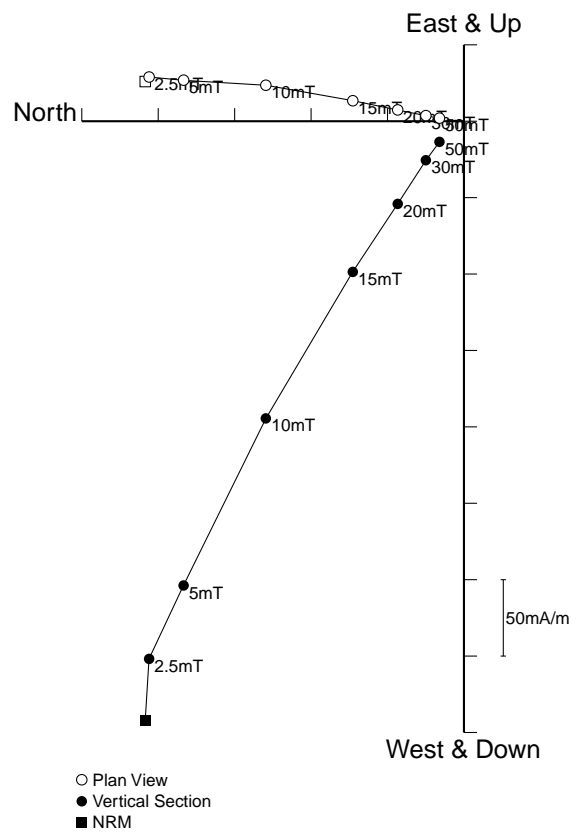
*Figure 10: Stepwise AF demagnetisation of sample 6BBP13. Diagram a) depicts the variation of the remanent direction as an equal area stereogram (declination increases clockwise, while inclination increases from zero at the equator to 90 degrees at the centre of the projection); b) shows the normalised change in remanence intensity as a function of the demagnetising field; c) shows the changes in both direction and intensity as a vector endpoint projection.*

*Figure 11: Comparison of the mean thermoremanent vector of samples 6BBP03, 6BBP06-8 and 6BBP10-16 after 5mT partial AF demagnetisation with the UK master calibration curve. Thick error bar lines represent 63% confidence limits and narrow lines 95% confidence limits.*
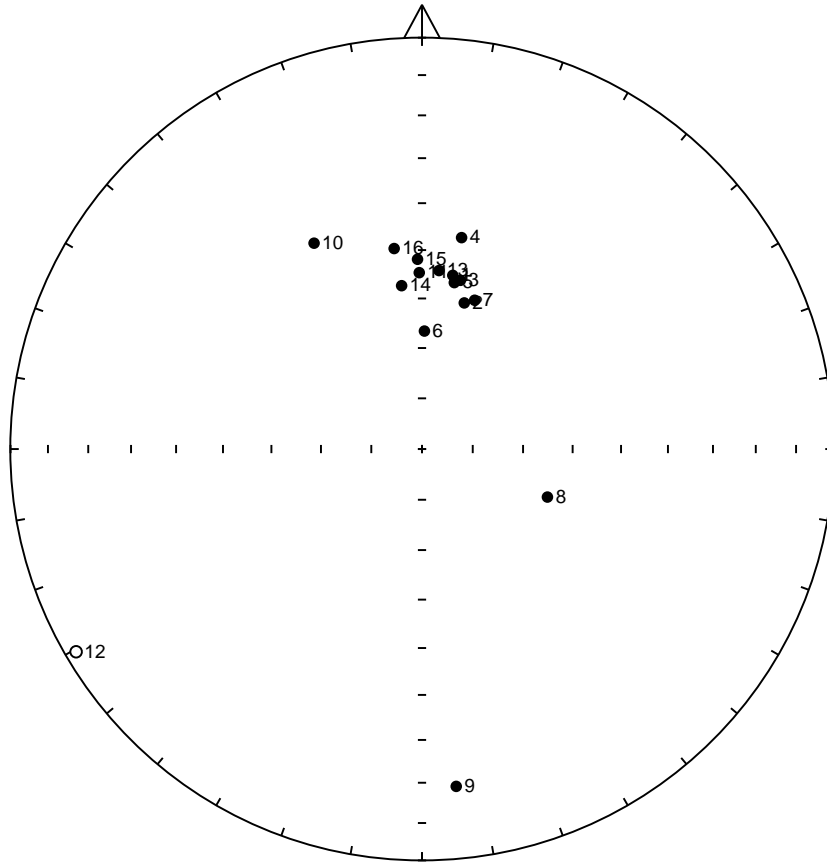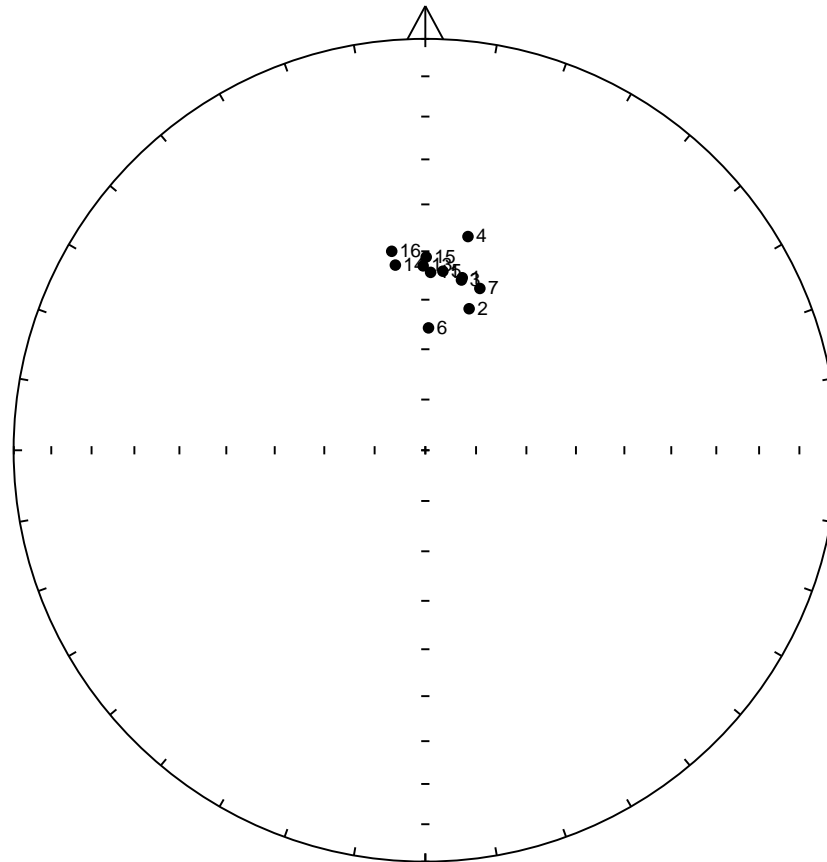
*Figure 12: a) Distribution of NRM directions of samples from feature 13ABP represented as an equal area stereogram. In this projection declination increases clockwise with zero being at 12 o'clock while inclination increases from zero at the equator to 90 degrees in the centre of the projection. Open circles represent negative inclinations. b) Distribution of thermoremanent directions of magnetisation of the same samples after partial AF demagnetisation to 5mT.*

*a)*

*b)*

Normalised Intensity $I/I_0$

*c)*

East & Up

North

West & Down

○ Plan View
● Vertical Section
■ NRM

100mA/m

Peak AF Demagnetising Field (mT)
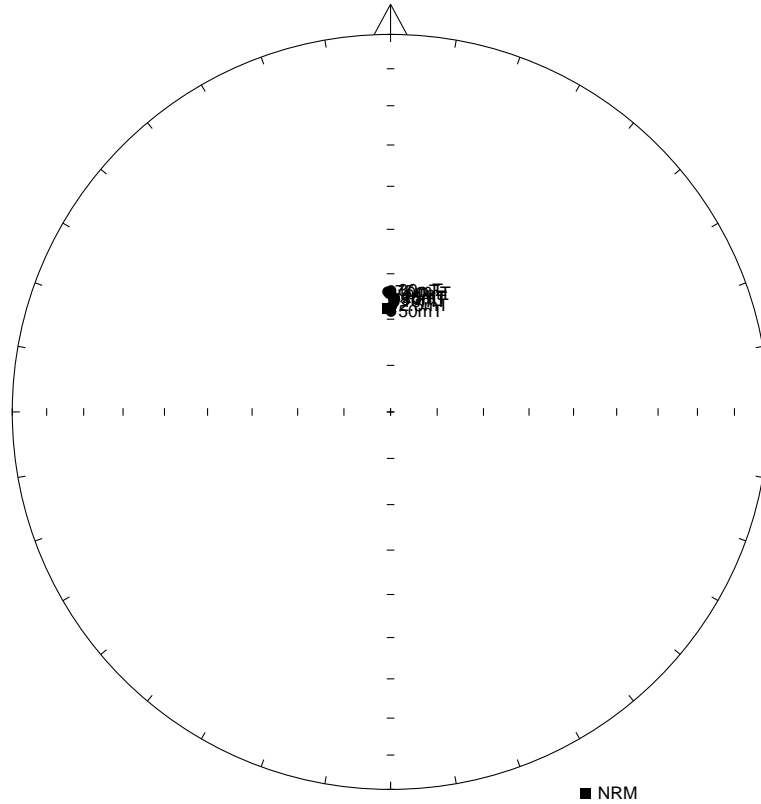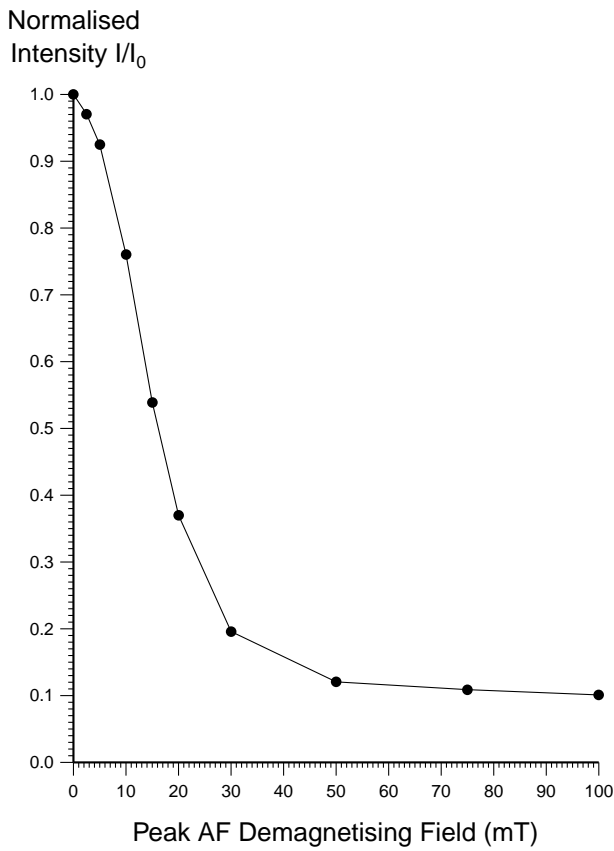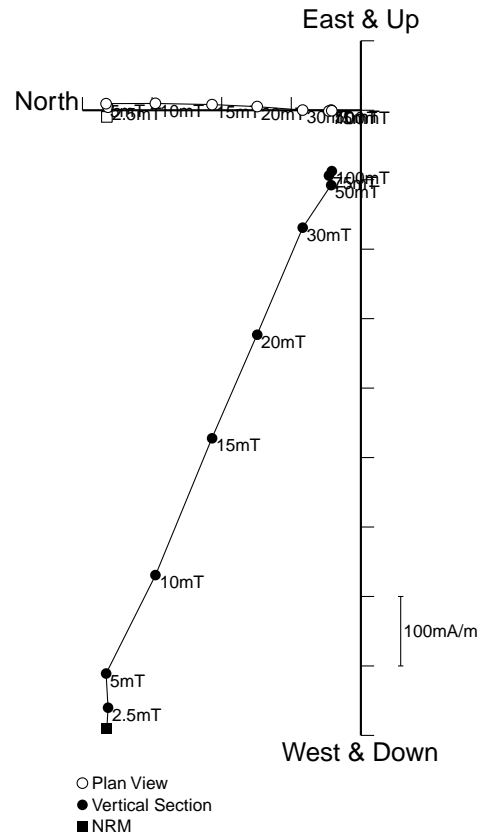
*Figure 13: Stepwise AF demagnetisation of sample 13ABP06. Diagram a) depicts the variation of the remanent direction as an equal area stereogram (declination increases clockwise, while inclination increases from zero at the equator to 90 degrees at the centre of the projection); b) shows the normalised change in remanence intensity as a function of the demagnetising field; c) shows the changes in both direction and intensity as a vector endpoint projection.*
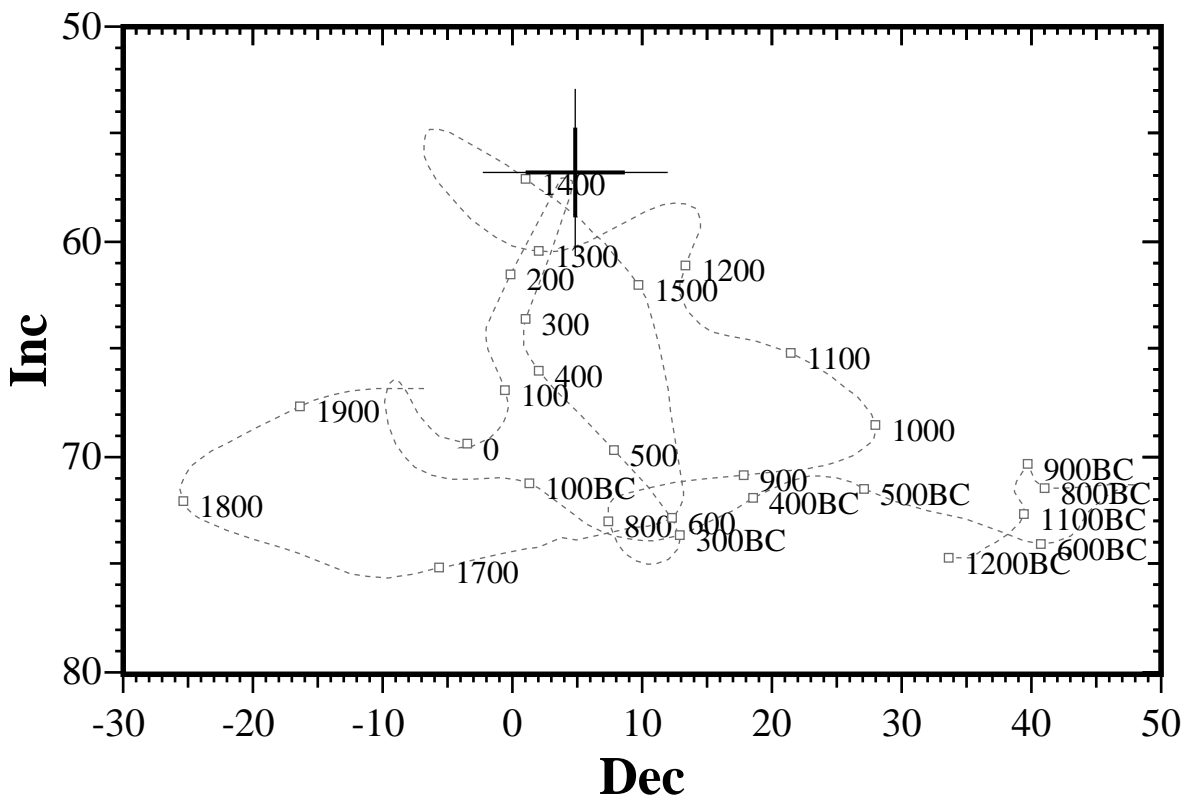
*Figure 14: Comparison of the mean thermoremanent vector of samples 13ABP01-7, 13ABP11 and 13ABP13-16 after 5mT partial AF demagnetisation with the UK master calibration curve. Thick error bar lines represent 63% confidence limits and narrow lines 95% confidence limits.*

*a)*
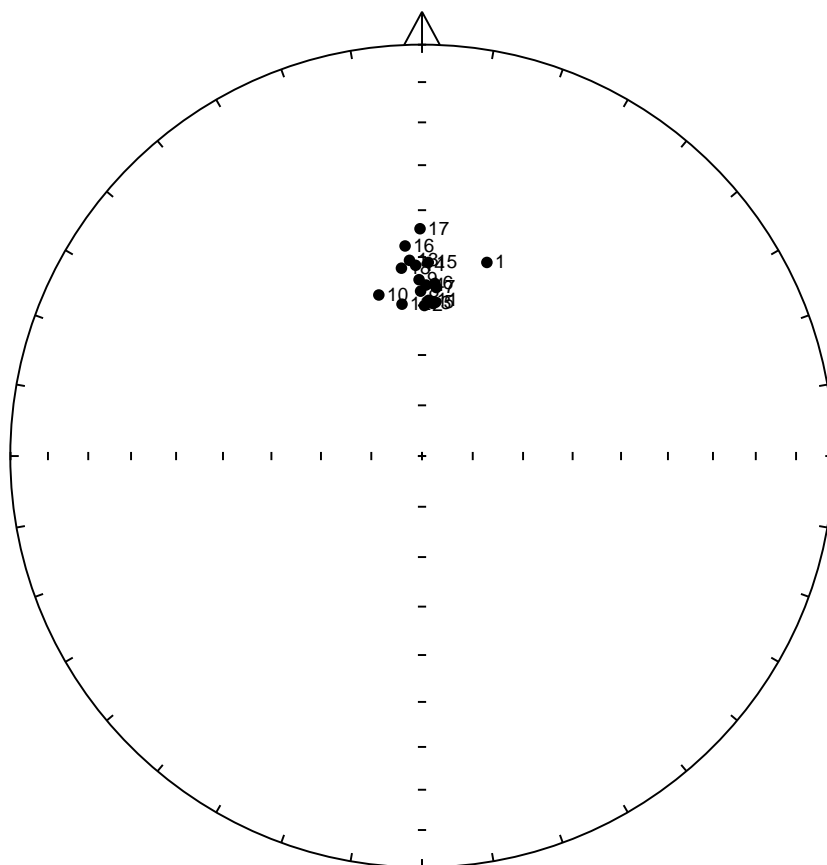
*b)*
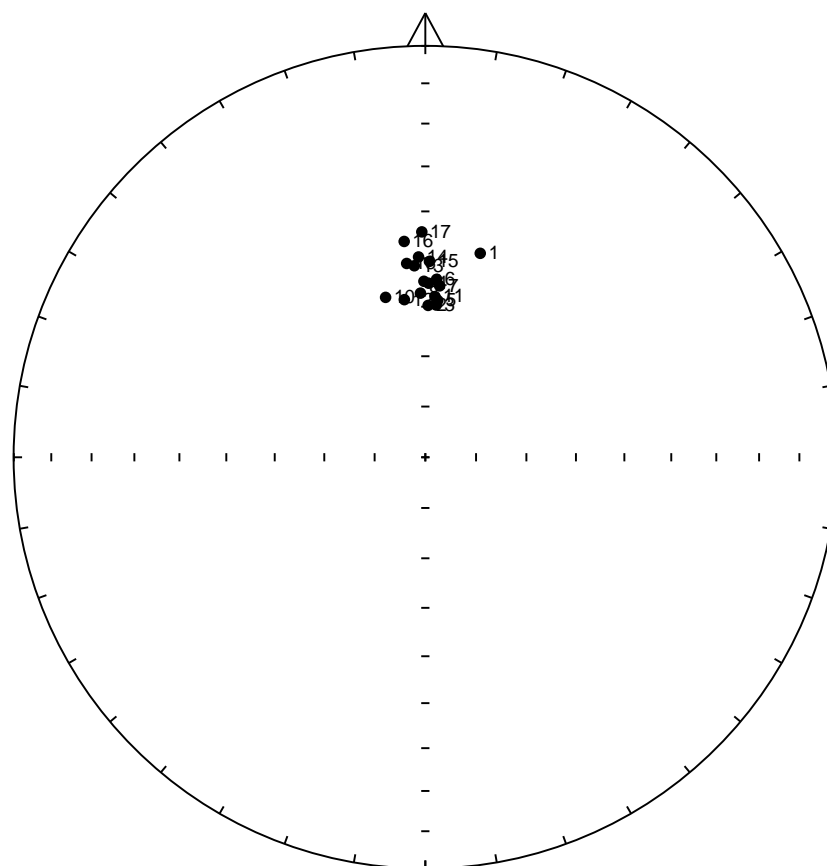
*Figure 15: a) Distribution of NRM directions of samples from feature 13BBP represented as an equal area stereogram. In this projection declination increases clockwise with zero being at 12 o'clock while inclination increases from zero at the equator to 90 degrees in the centre of the projection. Open circles represent negative inclinations. b) Distribution of thermoremanent directions of magnetisation of the same samples after partial AF demagnetisation to 10 or 50mT.*
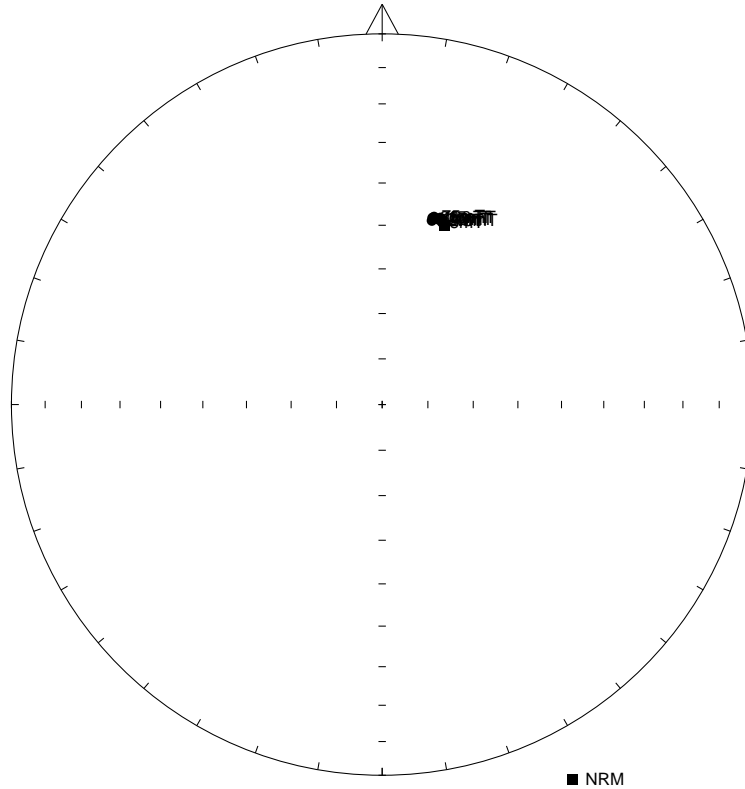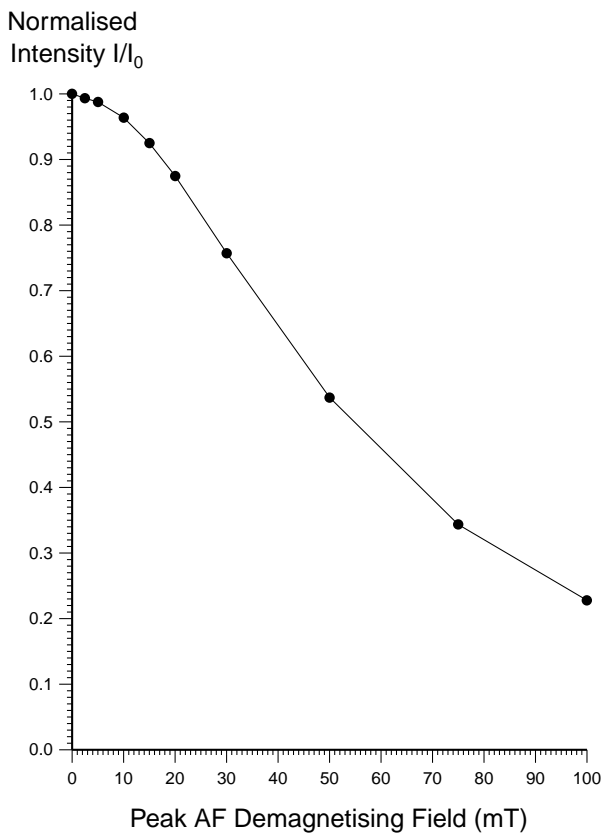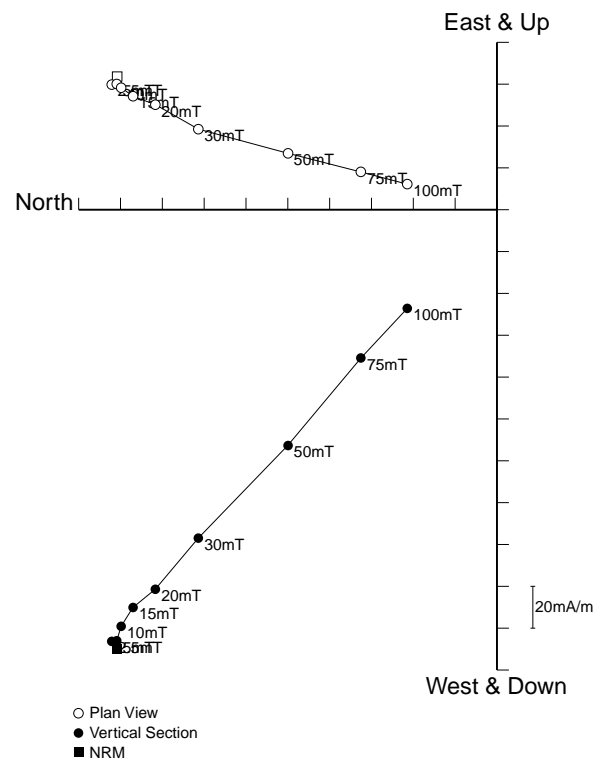
*Figure 16: Stepwise AF demagnetisation of sample 13BBP01. Diagram a) depicts the variation of the remanent direction as an equal area stereogram (declination increases clockwise, while inclination increases from zero at the equator to 90 degrees at the centre of the projection); b) shows the normalised change in remanence intensity as a function of the demagnetising field; c) shows the changes in both direction and intensity as a vector endpoint projection.*
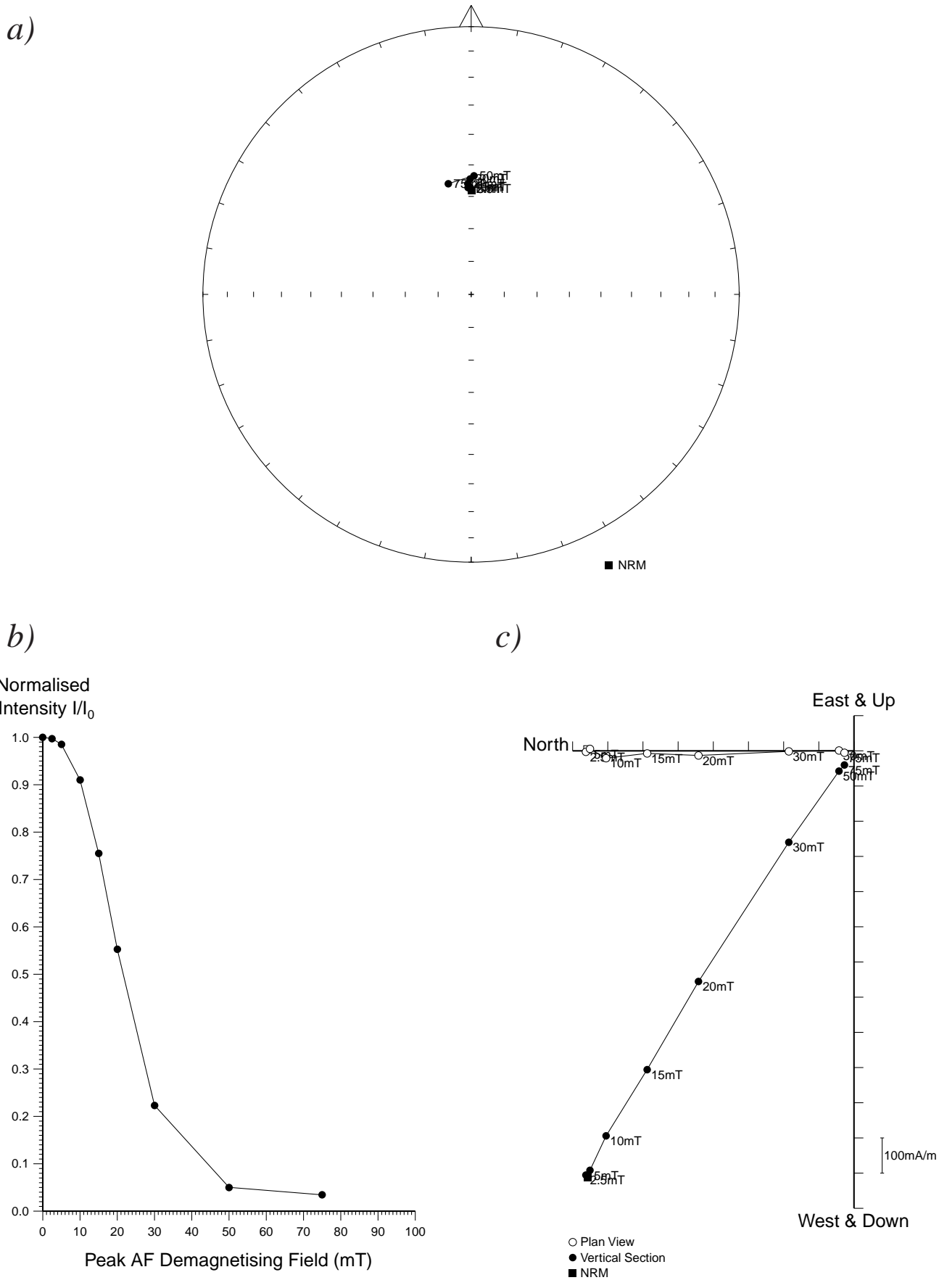
*Figure 17: Stepwise AF demagnetisation of sample 13BBP08. Diagram a) depicts the variation of the remanent direction as an equal area stereogram (declination increases clockwise, while inclination increases from zero at the equator to 90 degrees at the centre of the projection); b) shows the normalised change in remanence intensity as a function of the demagnetising field; c) shows the changes in both direction and intensity as a vector endpoint projection.*

34
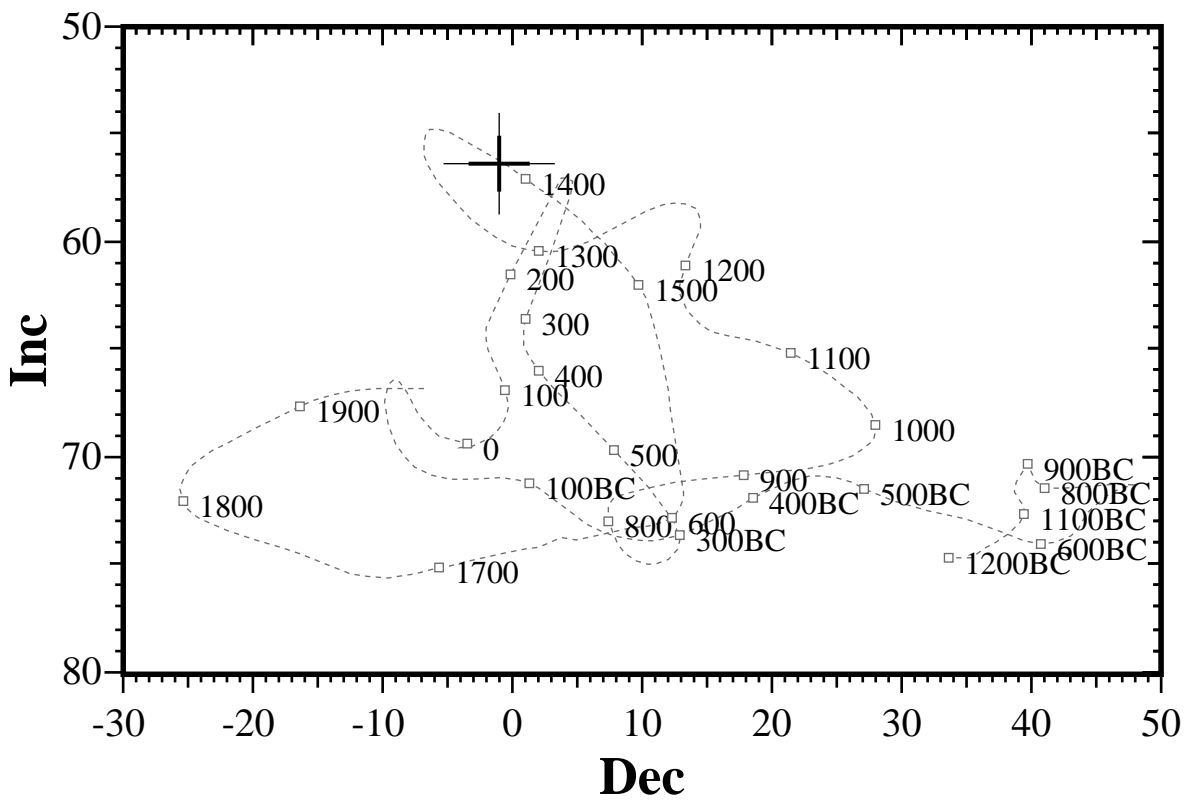
*Figure 18: Comparison of the mean thermoremanent vector of samples 13BBP02-18 after 10mT partial AF demagnetisation with the UK master calibration curve. Thick error bar lines represent 63% confidence limits and narrow lines 95% confidence limits.*

*a)*
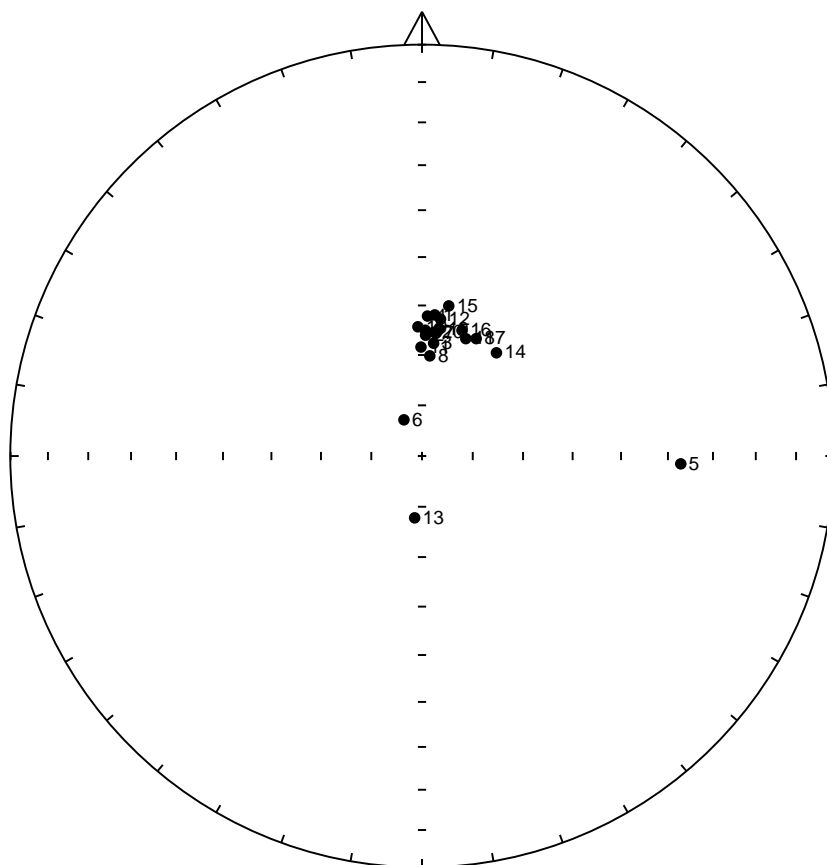


*b)*
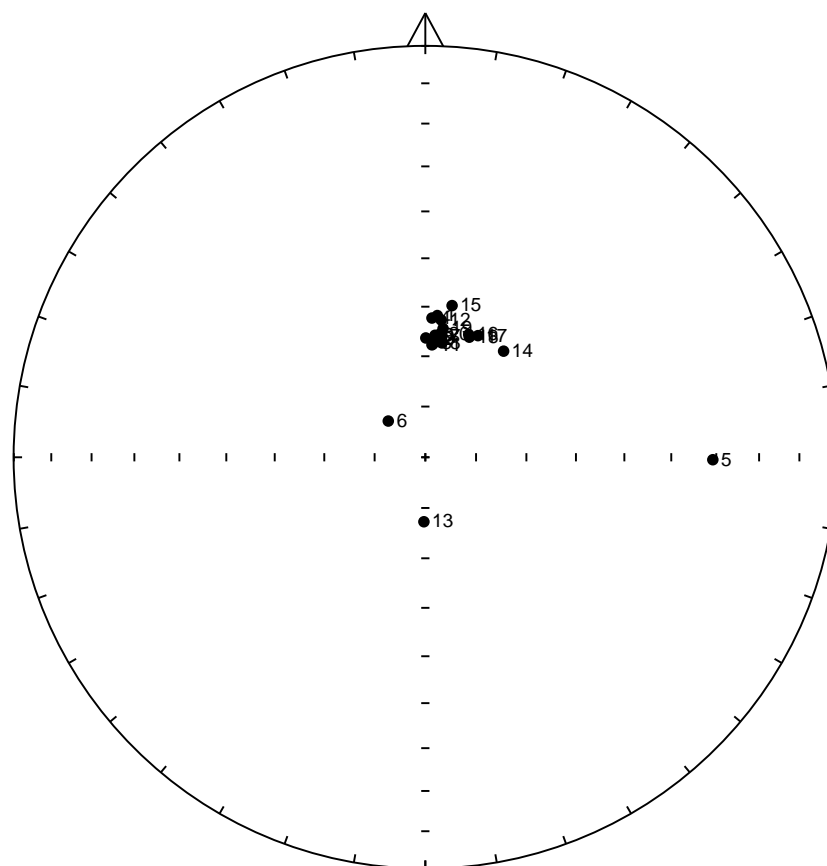


*Figure 19: a) Distribution of NRM directions of samples from feature 13CBP represented as an equal area stereogram. In this projection declination increases clockwise with zero being at 12 o'clock while inclination increases from zero at the equator to 90 degrees in the centre of the projection. Open circles represent negative inclinations. b) Distribution of thermoremanent directions of magnetisation of the same samples after partial AF demagnetisation to 10 or 50mT.*
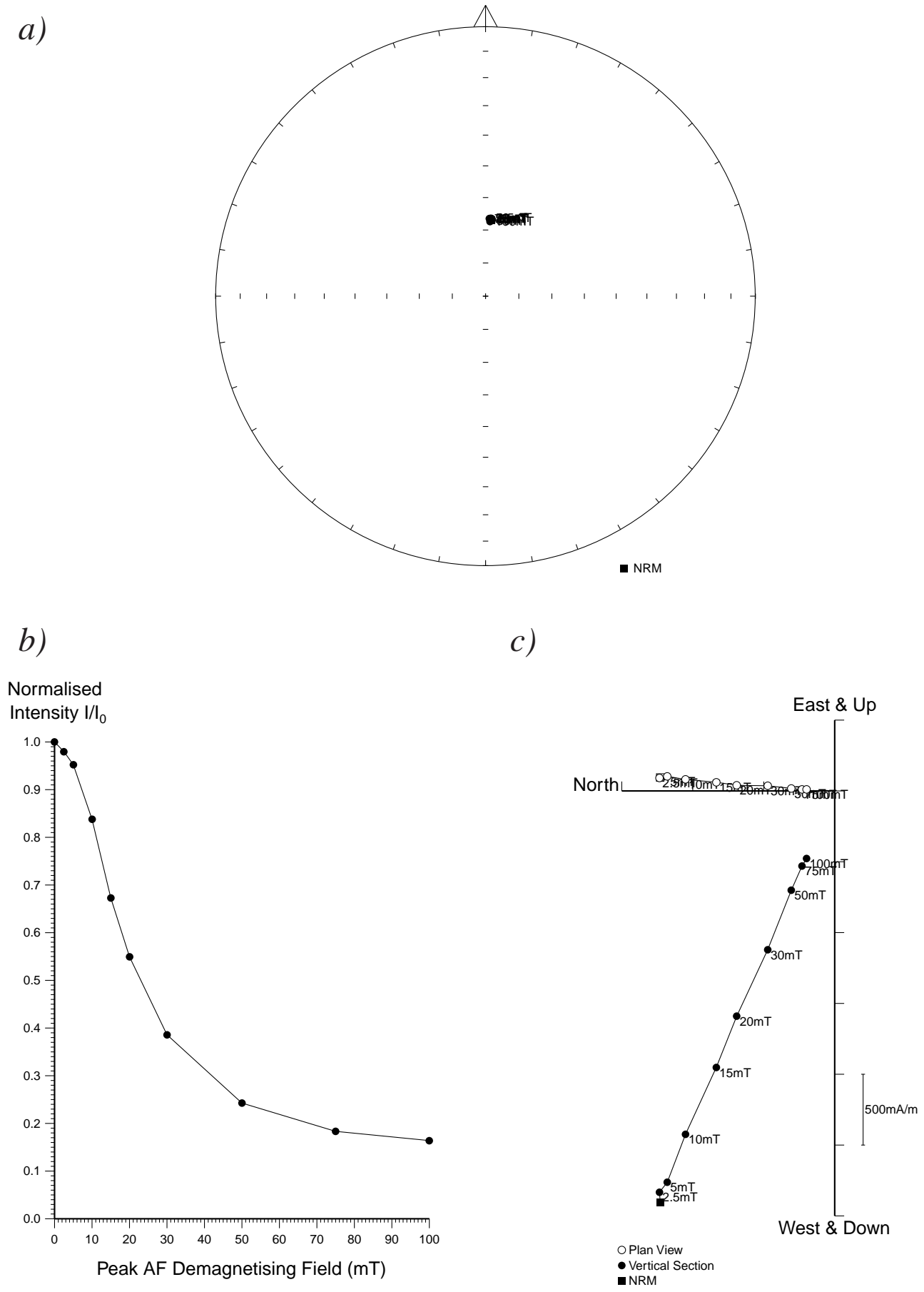
*Figure 20: Stepwise AF demagnetisation of sample 13CBP02. Diagram a) depicts the variation of the remanent direction as an equal area stereogram (declination increases clockwise, while inclination increases from zero at the equator to 90 degrees at the centre of the projection); b) shows the normalised change in remanence intensity as a function of the demagnetising field; c) shows the changes in both direction and intensity as a vector endpoint projection.*

*a)*

*b)*

Normalised
Intensity I/I₀

Peak AF Demagnetising Field (mT)

*c)*

East & Up

North

West & Down

○ Plan View
● Vertical Section
■ NRM

50mA/m
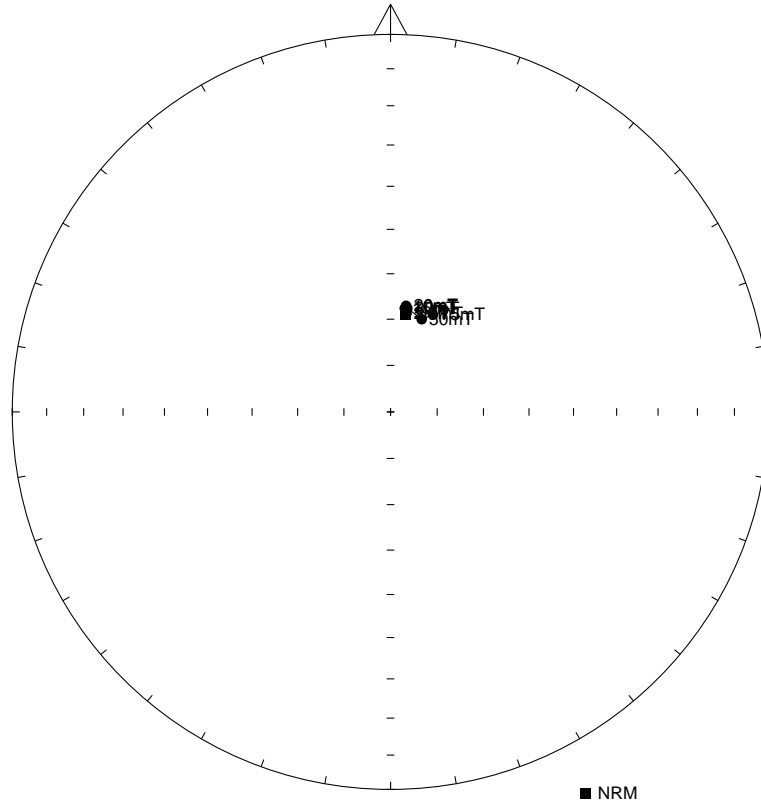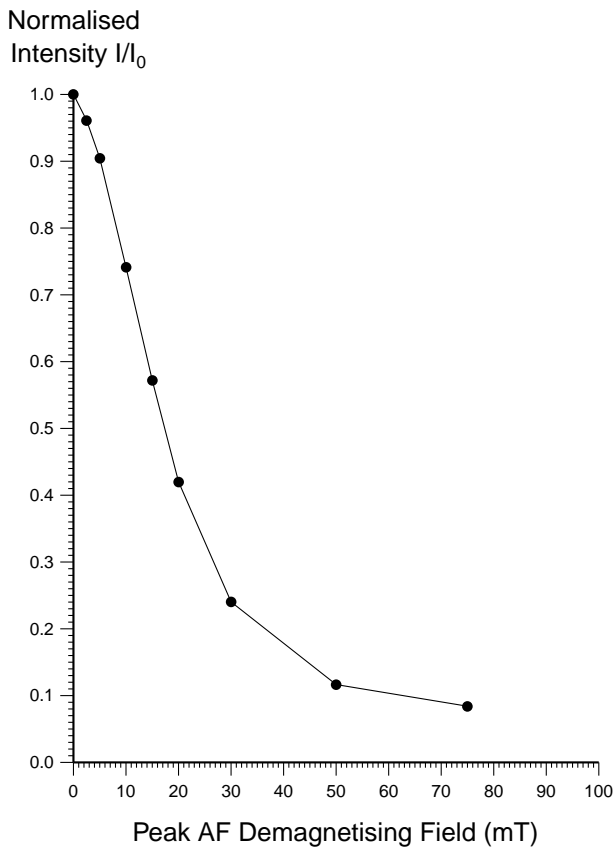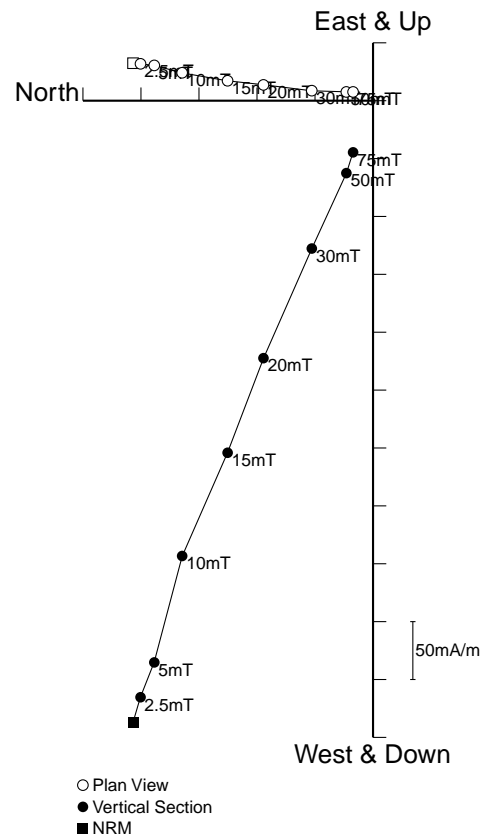
*Figure 21: Stepwise AF demagnetisation of sample 13CBP08. Diagram a) depicts the variation of the remanent direction as an equal area stereogram (declination increases clockwise, while inclination increases from zero at the equator to 90 degrees at the centre of the projection); b) shows the normalised change in remanence intensity as a function of the demagnetising field; c) shows the changes in both direction and intensity as a vector endpoint projection.*

*a)*

■ NRM

*b)*

Normalised
Intensity I/I$_0$

Peak AF Demagnetising Field (mT)

*c)*

East & Up

North

West & Down

○ Plan View
● Vertical Section
■ NRM

100mA/m
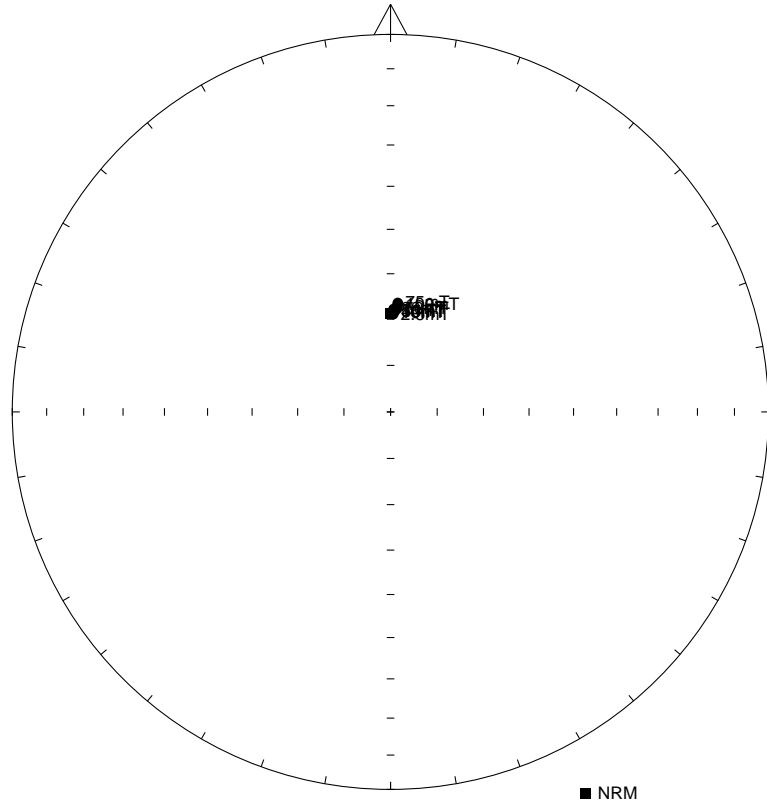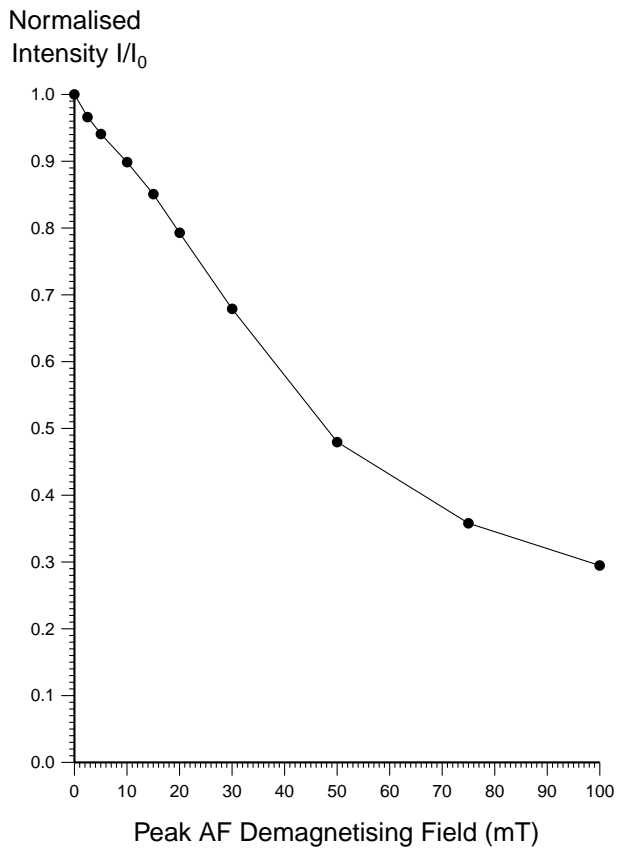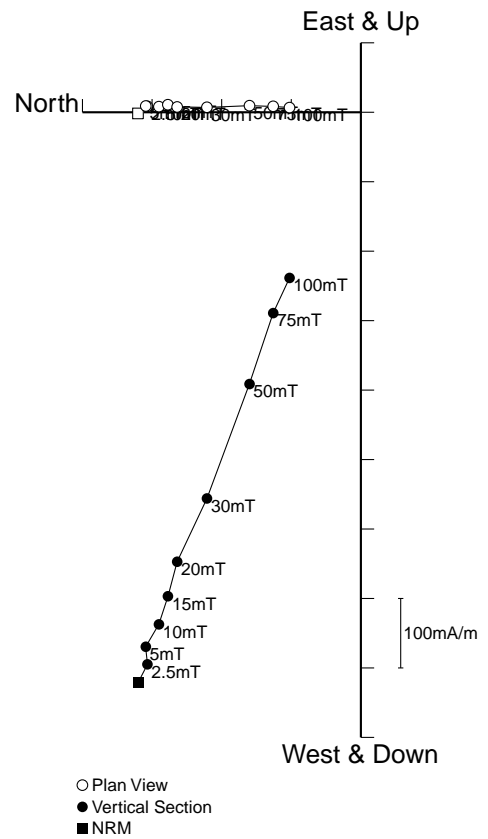
*Figure 22: Stepwise AF demagnetisation of sample 13CBP11. Diagram a) depicts the variation of the remanent direction as an equal area stereogram (declination increases clockwise, while inclination increases from zero at the equator to 90 degrees at the centre of the projection); b) shows the normalised change in remanence intensity as a function of the demagnetising field; c) shows the changes in both direction and intensity as a vector endpoint projection.*
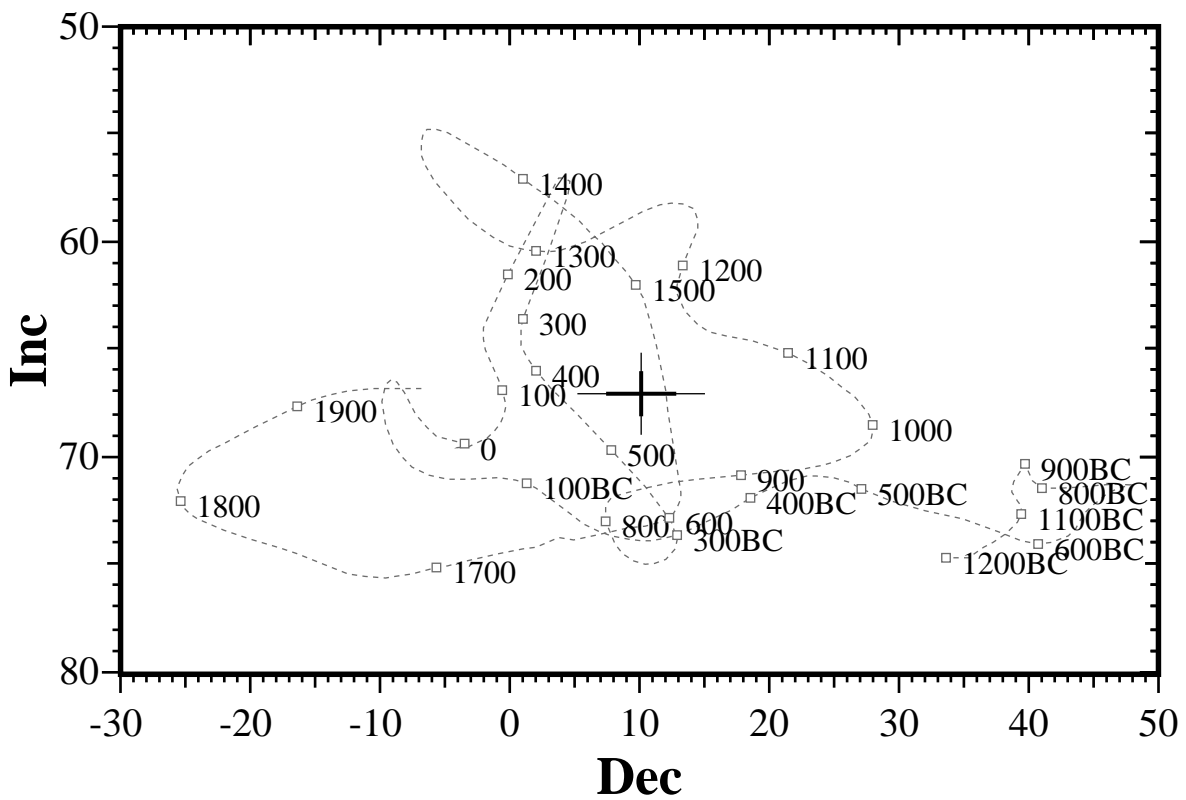
*Figure 23: Comparison of the mean thermoremanent vector of samples 13CBP01-4 and 13CBP07-20 after 10 or 50mT partial AF demagnetisation with the UK master calibration curve. Thick error bar lines represent 63% confidence limits and narrow lines 95% confidence limits.*

*a)*
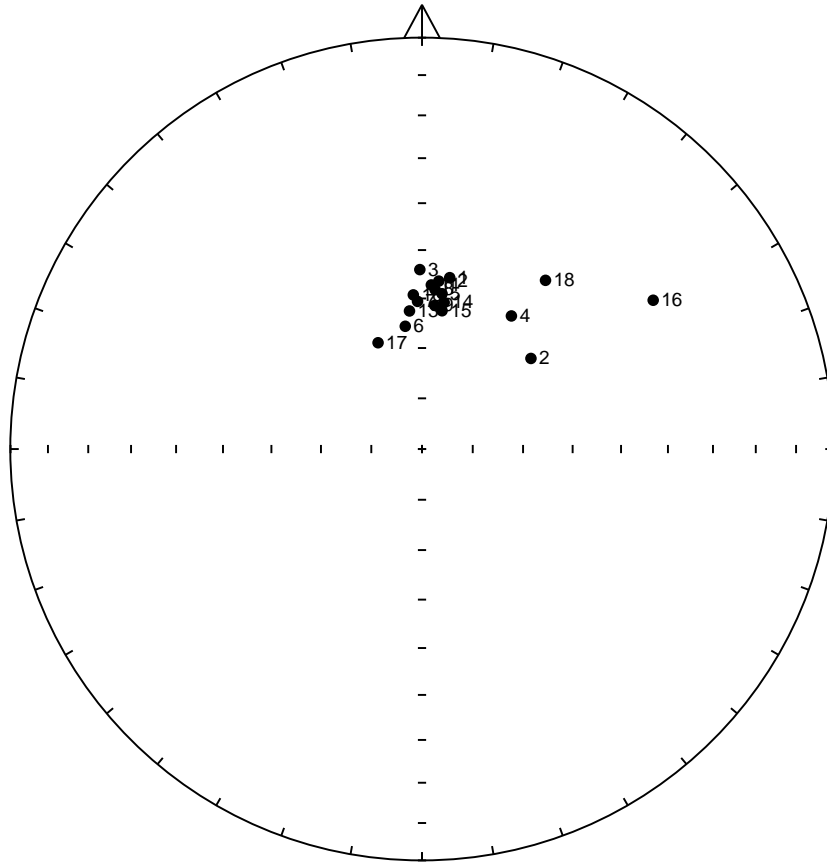


*b)*
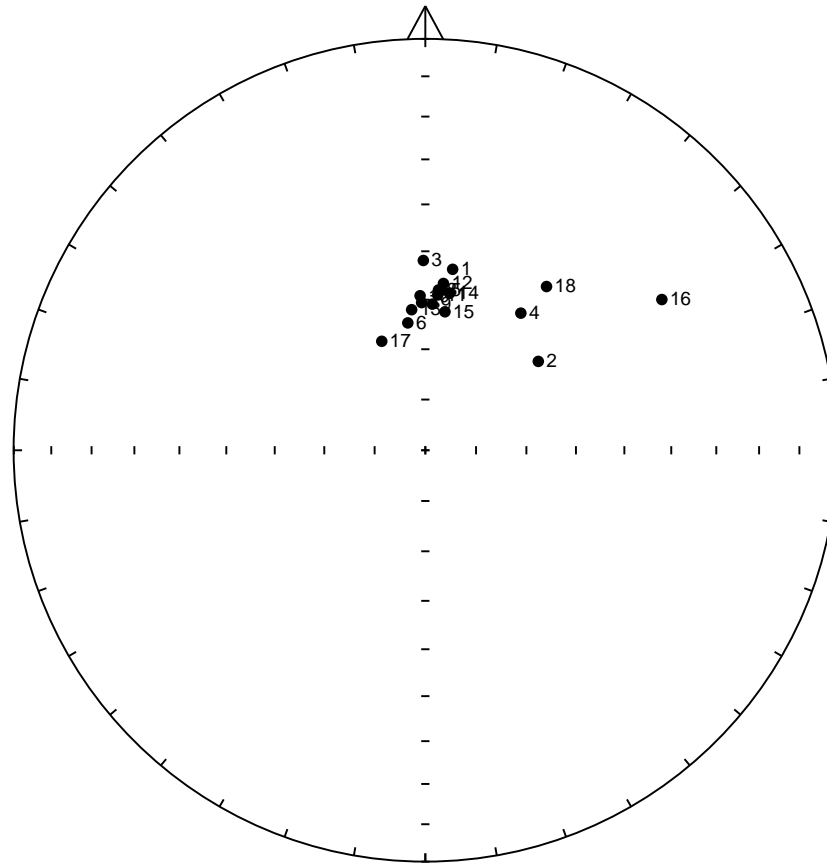


*Figure 24: a) Distribution of NRM directions of samples from feature 15ABP represented as an equal area stereogram. In this projection declination increases clockwise with zero being at 12 o'clock while inclination increases from zero at the equator to 90 degrees in the centre of the projection. Open circles represent negative inclinations. b) Distribution of thermoremanent directions of magnetisation of the same samples after partial AF demagnetisation to 10mT.*

*a)*



75mT
50mT
30mT
20mT

■ NRM

*b)*

Normalised
Intensity I/I$_0$

1.0

0.9

0.8

0.7

0.6

0.5

0.4

0.3

0.2

0.1

0.0

0  10  20  30  40  50  60  70  80  90  100

Peak AF Demagnetising Field (mT)

*c)*

East & Up

North

2.3m5mT
10m15m 20mT
30mT
50 5mT
75mT
50mT
30mT
20mT
15mT
10mT
5mT
2.5mT

500mA/m

West & Down

○ Plan View
● Vertical Section
■ NRM
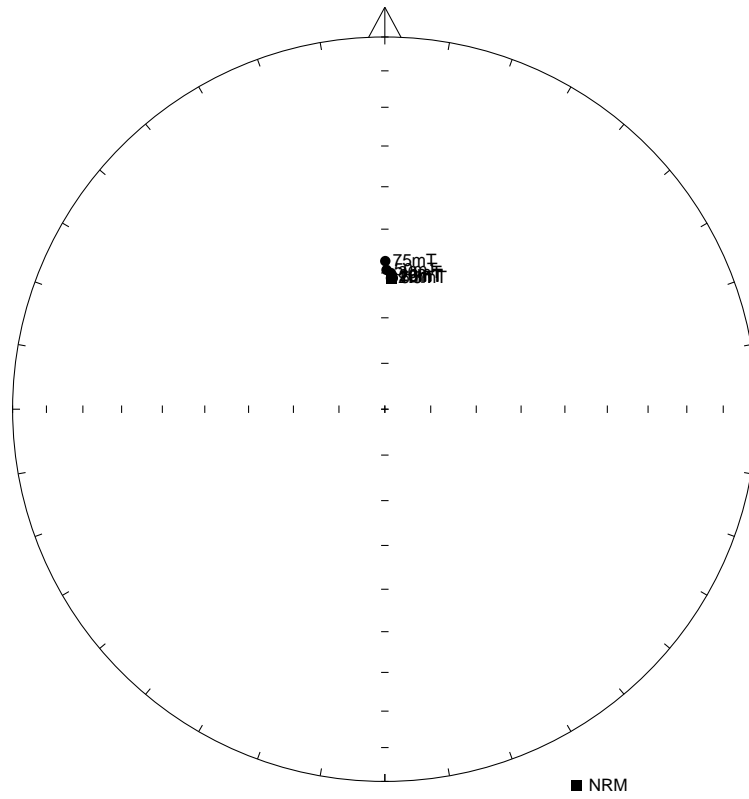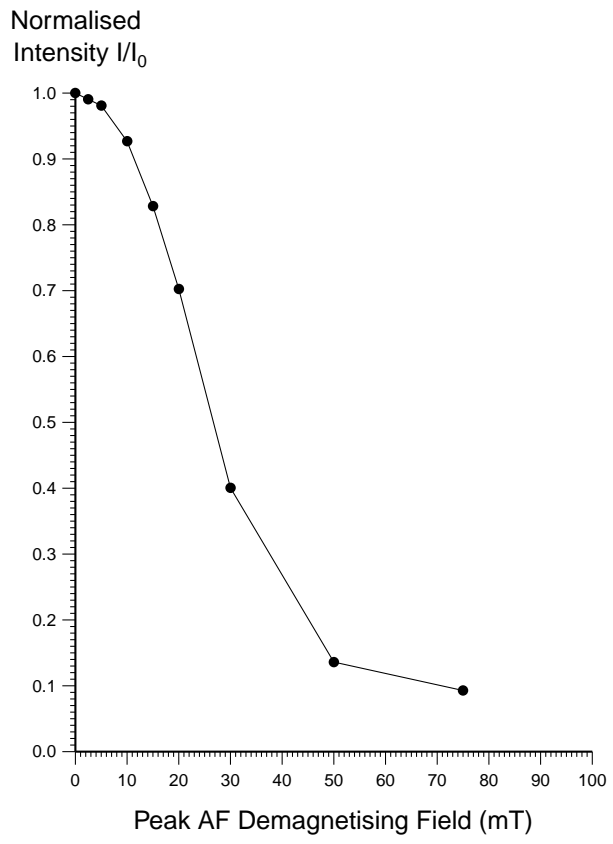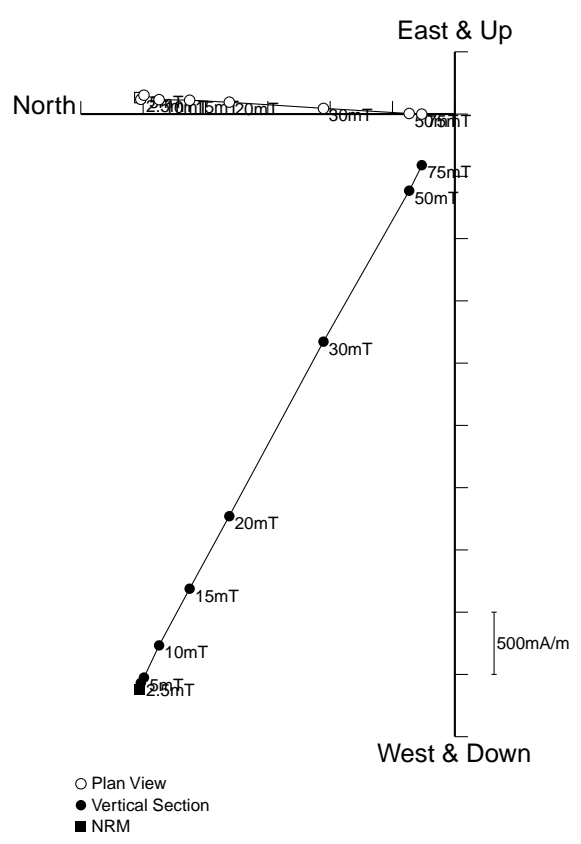
*Figure 25: Stepwise AF demagnetisation of sample 15ABP09. Diagram a) depicts the variation of the remanent direction as an equal area stereogram (declination increases clockwise, while inclination increases from zero at the equator to 90 degrees at the centre of the projection); b) shows the normalised change in remanence intensity as a function of the demagnetising field; c) shows the changes in both direction and intensity as a vector endpoint projection.*
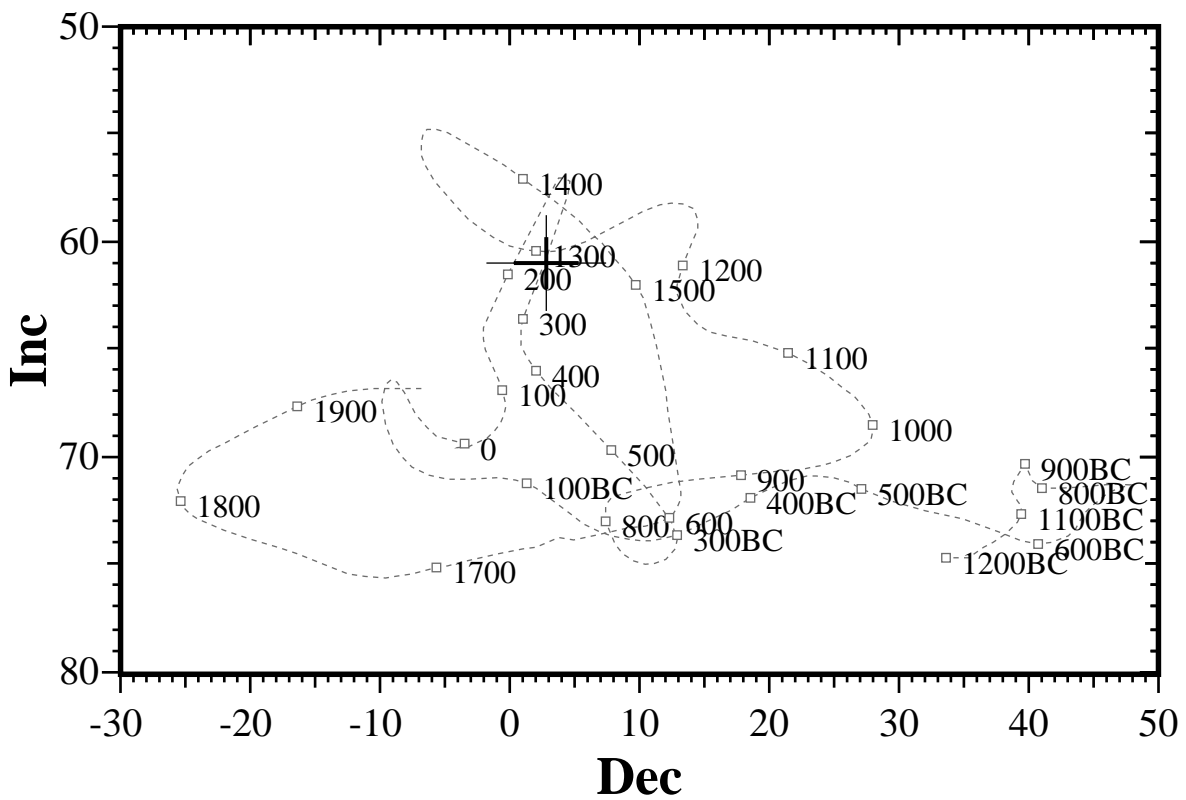
*Figure 26: Comparison of the mean thermoremanent vector of samples 15ABP01, 15ABP03 and 15ABP05-15 after 10mT partial AF demagnetisation with the UK master calibration curve. Thick error bar lines represent 63% confidence limits and narrow lines 95% confidence limits.*
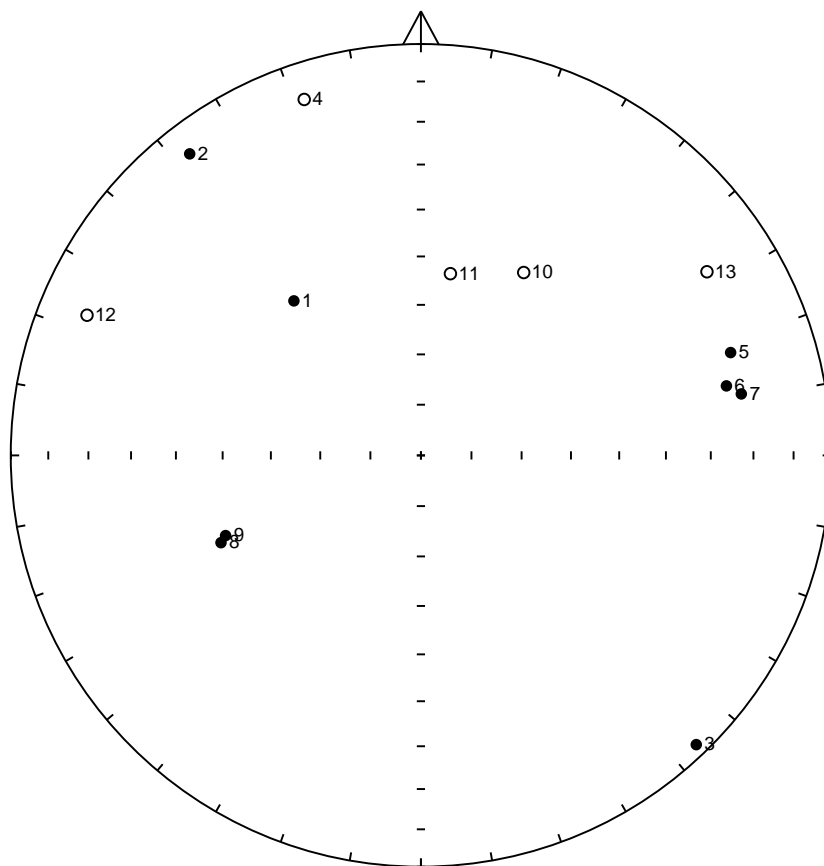
*Figure 27: Distribution of NRM directions of samples from feature 15BBP represented as an equal area stereogram. In this projection declination increases clockwise with zero being at 12 o'clock while inclination increases from zero at the equator to 90 degrees in the centre of the projection. Open circles represent negative inclinations.*